

Generalized density functional theory framework for the non-linear density response of quantum many-body systems

Zhandos A. Moldabekov,^{1,*} Cheng Ma,^{2,3} Xuecheng Shao,^{2,3,4} Sebastian Schwalbe,⁵
Pontus Svensson,¹ Panagiotis Tolias,⁶ Jan Vorberger,¹ and Tobias Dornheim^{1,5}

¹*Institute of Radiation Physics, Helmholtz-Zentrum Dresden-Rossendorf (HZDR), D-01328 Dresden, Germany*

²*Key Laboratory of Material Simulation Methods & Software of Ministry of Education,
College of Physics, Jilin University, Changchun 130012, China.*

³*State Key Lab of High Pressure and Superhard Materials,
College of Physics, Jilin University, Changchun 130012, China.*

⁴*International Center of Future Science, Jilin University, Changchun 130012, China.*

⁵*Center for Advanced Systems Understanding (CASUS) at*

Helmholtz-Zentrum Dresden-Rossendorf (HZDR), D-02826 Görlitz, Germany

⁶*Royal Institute of Technology (KTH) Stockholm, SE-100 44 Stockholm, Sweden*

A density functional theory (DFT) framework is presented that links functional derivatives of free-energy functionals to non-linear static density response functions in quantum many-body systems. Within this framework, explicit expressions are derived for various higher-order response functions of systems that are homogeneous on average, including the first theoretical result for the cubic response at the first harmonic $\chi_0^{(1,3)}(\mathbf{q})$. Specifically, our framework includes hitherto neglected mode-coupling effects that are important for the non-linear density response even in the presence of a single harmonic perturbation. We compare these predictions for $\chi_0^{(1,3)}(\mathbf{q})$ to new Kohn-Sham DFT simulations, leading to excellent agreement between theory and numerical results. Exact analytical expressions are also obtained for the long-wavelength limits of the ideal quadratic and cubic response functions. Particular emphasis is placed on the connections between the third- and fourth-order functional derivatives of the non-interacting free-energy functional $F_s[n]$ and the ideal quadratic and cubic response functions of the uniform electron gas, respectively. These relations provide exact constraints that may prove useful for the future construction of improved approximations to $F_s[n]$, in particular for warm dense matter applications at finite temperatures. Here, we use this framework to assess several commonly employed approximations to $F_s[n]$ through orbital-free DFT simulations of the harmonically perturbed ideal electron gas. The results are compared with Kohn-Sham DFT calculations across temperatures ranging from the ground state to the warm dense regime. Additionally, we analyze in detail the temperature- and wavenumber-dependent non-monotonic behavior of the ideal quadratic and cubic response functions.

I. INTRODUCTION

Density functional theory (DFT) is a powerful tool employed in both quantum and classical many-particle physics [1, 2]. It is widely used to understand and simulate materials across various phases. The relationship between the functional derivatives of different (free) energy functionals and density response functions connects DFT with other many-body theories, such as Green's functions and, more broadly, kinetic theory [3–5]. These approaches complement each other, enabling analysis from multiple viewpoints and a deeper understanding of the physics of many-body systems.

The connection between DFT and linear response theory is well established [6, 7]. In contrast, non-linear response theory within the DFT framework is much less explored [8]. Just as linear response theory has been crucial in advancing approximations for exchange-correlation (XC) functionals [9, 10], as well as non-interacting free-

energy and kinetic-energy functionals in density functional theory (DFT) [11], non-linear response theory can significantly enhance the quality of models and approximations in DFT. Additionally, as demonstrated here, the DFT framework enables us to identify general forms of solutions for non-linear response functions involving a hitherto unexplored and erroneously neglected mode-coupling mechanism that is important even in the presence of a single external perturbation. This can serve as a useful guide for more tedious theoretical approaches, such as the method of Green's functions and quantum kinetic theory [3, 12, 13]. Consequently, understanding the relationship between various types of energy functionals and non-linear response functions is essential for both the development of theory and the enhancement of DFT-based simulation methods.

In this work, we explore a general framework for DFT that links the functional derivatives of free-energy functionals to non-linear density response functions. This approach offers a straightforward way to identify how the coupling between different modes contributes to the non-linear response in different situations. We demonstrate this by providing the solution for the cubic response at

To the memory of Dr. Travis Edwin Sjostrom.

* z.moldabekov@hzdr.de

the first harmonic $\chi_0^{(1,3)}(\mathbf{q})$ (i.e., the leading non-linear term at the original perturbation [14, 15]) in terms of mode coupling between density perturbations at the first and second harmonics. This solution, long obscured and overlooked in the intricacies of Green's functions [3] and quantum-kinetic [12] analyses, emerges here with surprising clarity. As a benchmark for future theoretical developments, we provide exact data for $\chi_0^{(1,3)}(\mathbf{q})$ computed by Kohn-Sham (KS) DFT simulations of the harmonically perturbed ideal uniform electron gas (UEG). Additionally, we derive the exact analytical solution for the long-wavelength limit of $\chi_0^{(1,3)}(\mathbf{q})$ of the UEG.

We employ the developed framework to evaluate the performance of commonly used non-interacting free-energy functional approximations in describing the non-linear density response of the UEG across temperatures spanning from the ground state to the high-temperature regime. We consider the ground-state Wang-Teter (WT) functional [16] and its finite-temperature version developed by Sjöström and Daligault [17], which is conventionally referred to as the WTF functional. Additionally, we examine the generalized gradient approximation (GGA) introduced by Luo, Karasiev, and Trickey, denoted as LKTF [18, 19]. Lastly, we discuss the recently proposed fully nonlocal functional by Ma et al. [20, 21], referred to as XWMF. The discussion of the results primarily focuses on warm dense matter (WDM) applications, a state of matter characterized by the simultaneous importance of strong thermal excitations, quantum degeneracy effects, and interparticle correlations [5, 22–27]; see Ref. [28] for a topical WDM roadmap article.

Because orbital-free methods rely heavily on the UEG limit, the accuracy of the non-interacting free-energy functional in this regime is critical for modeling metals, semiconductors, and quantum plasmas [11, 18, 26, 29–31]. The presented analysis can be particularly valuable for the development of new non-interacting free-energy functionals at conditions where accurate modeling of the electronic screening of ion-ion pair interaction is crucial. In this regard, we highlight the previously overlooked fact that the non-interacting free energy functional, which can reproduce the known limit of the ideal linear density response function of the UEG—specifically the Lindhard function [32] (e.g., Wang-Teter-type functionals [16, 17])—should also automatically reproduce the established analytical solution for the quadratic density response function at the second harmonic $\chi_0^{(2)}(\mathbf{q})$ [33]. This is because $\chi_0^{(2)}(\mathbf{q})$ is fully defined in terms of the ideal linear density response function. The same principle applies to higher-order response functions at higher harmonics (the l -order ideal density response at the l th harmonic [12]), although these become progressively less significant as l increases.

Finally, our results complement a series of earlier works on the non-linear density response of the UEG and related systems [3–5, 8, 12, 15, 33–39], which is important in its own right.

The paper is organized as follows: In Sec. II, we present the theory of non-linear response within the framework of DFT. Sec. III applies this developed theory to analyze non-interacting free energy functionals and examines the behavior of the exact solutions for the ideal non-linear density response functions of the UEG across different parameters. We conclude the paper by summarizing the main findings and providing an outlook on future applications of the presented framework.

II. THEORY

A. General Framework

We start from the free-energy functional of electrons as it is considered in DFT:

$$F[n] = F_s[n] + F_H[n] + F_{xc}[n] + \int d\mathbf{r} v_{\text{ext}}(\mathbf{r}) n(\mathbf{r}), \quad (1)$$

where $F_s[n]$ is the non-interacting free energy functional, $F_H[n]$ is the contribution due to Hartree mean field, $F_{xc}[n]$ is the contribution due to exchange-correlation effects, and v_{ext} is an external potential, e.g., due to ions, nuclei and externally applied fields.

For the equilibrium state, we have:

$$\frac{\delta F_s}{\delta n(\mathbf{r})} + \frac{\delta F_H}{\delta n(\mathbf{r})} + \frac{\delta F_{xc}}{\delta n(\mathbf{r})} + v_{\text{ext}}(\mathbf{r}) = \mu, \quad (2)$$

with μ being the chemical potential playing the role of the Lagrangian multiplier that enforces the particle number conservation [11].

In Eq. (2), it is convenient to define the potentials:

$$v_s(\mathbf{r}) \equiv \frac{\delta F_s}{\delta n(\mathbf{r})}, \quad v_H(\mathbf{r}) \equiv \frac{\delta F_H}{\delta n(\mathbf{r})}, \quad v_{xc}(\mathbf{r}) \equiv \frac{\delta F_{xc}}{\delta n(\mathbf{r})}. \quad (3)$$

Now, we perturb the initial equilibrium state by applying an external perturbation and consider the change in density Δn , potentials (Δv_s etc.), and chemical potential $\Delta\mu$:

$$\Delta v_s(\mathbf{r}) + \Delta v_H(\mathbf{r}) + \Delta v_{xc}(\mathbf{r}) + \Delta v_{\text{ext}}(\mathbf{r}) = \Delta\mu. \quad (4)$$

We consider a periodic system of volume $\Omega = L^3$ with reciprocal lattice vectors \mathbf{k} . The discrete Fourier components are

$$\Delta v(\mathbf{r}) = \frac{1}{\Omega} \sum_{\mathbf{k}} e^{i\mathbf{k}\cdot\mathbf{r}} \Delta v(\mathbf{k}), \quad \Delta v(\mathbf{k}) = \int_{\Omega} d\mathbf{r} e^{-i\mathbf{k}\cdot\mathbf{r}} \Delta v(\mathbf{r}), \quad (5)$$

and

$$\int_{\Omega} d\mathbf{r} e^{i(\mathbf{k}-\mathbf{k}')\cdot\mathbf{r}} = \Omega \delta_{\mathbf{k},\mathbf{k}'}, \quad (6)$$

where $\delta_{\mathbf{k},\mathbf{k}'}$ is the Kronecker delta on the discrete reciprocal lattice.

With these conventions, the Fourier transform of Eq. (4) gives:

$$\Delta v_s(\mathbf{k}) + \Delta v_H(\mathbf{k}) + \delta v_{xc}(\mathbf{k}) + \Delta v_{ext}(\mathbf{k}) = \Delta\mu \Omega \delta_{\mathbf{k},0}, \quad (7)$$

where $\Delta\mu \delta_{\mathbf{k},0}$ only matters in the case $\mathbf{k} = 0$, and for $\mathbf{k} \neq 0$ we set the r.h.s. of Eq. (7) to zero. The particle

number conservation $\int d\mathbf{r} \Delta n(\mathbf{r}) = 0$ is enforced by tuning $\Delta\mu$, which is a number representing the change in the chemical potential.

We perform a functional Taylor expansion of each potential in powers of Δn . For example, for $\Delta v_s(\mathbf{r})$ we write:

$$\begin{aligned} \Delta v_s(\mathbf{r}) = & \int d\mathbf{r}_1 \mathcal{K}_s^{(2)}(\mathbf{r}, \mathbf{r}_1) \Delta n(\mathbf{r}_1) + \iint d\mathbf{r}_1 d\mathbf{r}_2 \mathcal{K}_s^{(3)}(\mathbf{r}, \mathbf{r}_1, \mathbf{r}_2) \Delta n(\mathbf{r}_1) \Delta n(\mathbf{r}_2) \\ & + \iiint d\mathbf{r}_1 d\mathbf{r}_2 d\mathbf{r}_3 \mathcal{K}_s^{(4)}(\mathbf{r}, \mathbf{r}_1, \mathbf{r}_2, \mathbf{r}_3) \Delta n(\mathbf{r}_1) \Delta n(\mathbf{r}_2) \Delta n(\mathbf{r}_3) + \dots \end{aligned} \quad (8)$$

where the l -th order functional derivative of $F_s[n]$ around the equilibrium density n_0 is denoted as:

$$\mathcal{K}_s^{(l)}(\mathbf{r}, \mathbf{r}_1, \dots, \mathbf{r}_{l-1}) \equiv \frac{\delta^{(l)} F_s}{\delta n(\mathbf{r}) \delta n(\mathbf{r}_1) \dots \delta n(\mathbf{r}_{l-1})} \Big|_{n_0}. \quad (9)$$

Similarly, we define the functional derivatives of the XC functional:

$$\mathcal{K}_{xc}^{(l)}(\mathbf{r}, \mathbf{r}_1, \dots, \mathbf{r}_{l-1}) \equiv \frac{\delta^{(l)} F_s}{\delta n(\mathbf{r}) \delta n(\mathbf{r}_1) \dots \delta n(\mathbf{r}_{l-1})} \Big|_{n_0}. \quad (10)$$

Further, for an l -th order kernel $\mathcal{K}^{(l)}(\mathbf{r}, \mathbf{r}_1, \dots, \mathbf{r}_{l-1})$ defined in a periodic cell of volume Ω , we associate reciprocal vectors $\mathbf{k}, \mathbf{k}_1, \dots, \mathbf{k}_{l-1}$ to the coordinates $\mathbf{r}, \mathbf{r}_1, \dots, \mathbf{r}_{l-1}$, respectively, and define the Fourier transform:

$$\begin{aligned} \mathcal{K}^{(l)}(\mathbf{k}, \mathbf{k}_1, \dots, \mathbf{k}_{l-1}) = & \int_{\Omega} d\mathbf{r} \int_{\Omega} d\mathbf{r}_1 \dots \int_{\Omega} d\mathbf{r}_{l-1} e^{-i\mathbf{k}\cdot\mathbf{r}} \prod_{j=1}^{l-1} [e^{+i\mathbf{k}_j\cdot\mathbf{r}_j}] \mathcal{K}(\mathbf{r}, \mathbf{r}_1, \dots, \mathbf{r}_{l-1}). \end{aligned} \quad (11)$$

Next, we explicitly assume a homogeneous system as it is realized in disordered materials [26, 40] (i.e., no crystal lattice). Due to translational invariance, one can introduce reduced kernels:

$$\mathcal{K}^{(l)}(\mathbf{k}, \mathbf{k}_1, \dots, \mathbf{k}_{l-1}) = \Omega \delta_{\mathbf{k}, \mathbf{k}_1 + \dots + \mathbf{k}_{l-1}} \tilde{\mathcal{K}}^{(l)}(\mathbf{k}_1, \dots, \mathbf{k}_{l-1}). \quad (12)$$

In Eq. (12), let us refer to \mathbf{k} as the “output” wavevector, and to $\{\mathbf{k}_1, \dots, \mathbf{k}_l\}$ as the “input” wavevectors. Furthermore, for bookkeeping purposes, we explicitly indicate in the reduced kernels the “output” wavevector by introducing the following notation for the kernels with $l > 2$:

$$\tilde{\mathcal{K}}^{(l)}(\mathbf{k}_1, \dots, \mathbf{k}_{l-1}) = \tilde{\mathcal{K}}^{(l)}(\mathbf{k} | \mathbf{k}_1, \dots, \mathbf{k}_{l-1}), \quad (13)$$

which simply means that the “input” wavevectors in the reduced kernels satisfy the momentum conservation $\mathbf{k} = \mathbf{k}_1 + \dots + \mathbf{k}_{l-1}$. This notation allows one to group density response terms by harmonics (in accordance with Eq. (27)) in a transparent way.

With these notations, a Fourier transform $\Delta v^{(l)}(\mathbf{k})$ of the l -th order term $\Delta v^{(l)}(\mathbf{r})$, in the expansions such as Eq. (8), can now be expressed as

$$\Delta v^{(l)}(\mathbf{k}) \equiv \frac{1}{\Omega^{l-2}} \sum_{\substack{\mathbf{k}_1, \dots, \mathbf{k}_{l-1} \\ \mathbf{k} = \mathbf{k}_1 + \dots + \mathbf{k}_{l-1}}} \tilde{\mathcal{K}}^{(l)}(\mathbf{k} | \mathbf{k}_1, \dots, \mathbf{k}_{l-1}) \Delta n(\mathbf{k}_1) \dots \Delta n(\mathbf{k}_{l-1}), \quad (14)$$

where we set $l \geq 2$ to align with the order of the functional derivatives in the kernels of the expansion, and used the notation $\sum_{\substack{\mathbf{k}_1, \dots, \mathbf{k}_{l-1} \\ \mathbf{k} = \mathbf{k}_1 + \dots + \mathbf{k}_{l-1}}}$ meaning that the sum is taken only

over those sets of momenta $\mathbf{k}_1, \dots, \mathbf{k}_{l-1}$ whose total momentum equals the “input” momentum \mathbf{k} . This enforces the momentum-conserving condition $\mathbf{k} = \mathbf{k}_1 + \dots + \mathbf{k}_{l-1}$.

Fourier transforming and using Eq. (14), for the functional Taylor expansions of the potential Δv_s and Δv_{xc} , we can write:

$$\begin{aligned}
\Delta v_s(\mathbf{k}) &= \tilde{\mathcal{K}}_s^{(2)}(\mathbf{k}) \Delta n(\mathbf{k}) \\
&+ \frac{1}{\Omega} \sum_{\substack{\mathbf{k}_1, \mathbf{k}_2 \\ \mathbf{k}=\mathbf{k}_1+\mathbf{k}_2}} \tilde{\mathcal{K}}_s^{(3)}(\mathbf{k}|\mathbf{k}_1, \mathbf{k}_2) \Delta n(\mathbf{k}_1) \Delta n(\mathbf{k}_2) \\
&+ \frac{1}{\Omega^2} \sum_{\substack{\mathbf{k}_1, \mathbf{k}_2, \mathbf{k}_3 \\ \mathbf{k}=\mathbf{k}_1+\mathbf{k}_2+\mathbf{k}_3}} \tilde{\mathcal{K}}_s^{(4)}(\mathbf{k}|\mathbf{k}_1, \mathbf{k}_2, \mathbf{k}_3) \Delta n(\mathbf{k}_1) \Delta n(\mathbf{k}_2) \Delta n(\mathbf{k}_3) \\
&+ \dots,
\end{aligned} \tag{15}$$

and

$$\begin{aligned}
\Delta v_{xc}(\mathbf{k}) &= \tilde{\mathcal{K}}_{xc}^{(2)}(\mathbf{k}) \Delta n(\mathbf{k}) \\
&+ \frac{1}{\Omega} \sum_{\substack{\mathbf{k}_1, \mathbf{k}_2 \\ \mathbf{k}=\mathbf{k}_1+\mathbf{k}_2}} \tilde{\mathcal{K}}_{xc}^{(3)}(\mathbf{k}|\mathbf{k}_1, \mathbf{k}_2) \Delta n(\mathbf{k}_1) \Delta n(\mathbf{k}_2) \\
&+ \frac{1}{\Omega^2} \sum_{\substack{\mathbf{k}_1, \mathbf{k}_2, \mathbf{k}_3 \\ \mathbf{k}=\mathbf{k}_1+\mathbf{k}_2+\mathbf{k}_3}} \tilde{\mathcal{K}}_{xc}^{(4)}(\mathbf{k}|\mathbf{k}_1, \mathbf{k}_2, \mathbf{k}_3) \Delta n(\mathbf{k}_1) \Delta n(\mathbf{k}_2) \Delta n(\mathbf{k}_3) \\
&+ \dots,
\end{aligned} \tag{16}$$

Note that $\tilde{\mathcal{K}}_{xc}^{(2)}(\mathbf{k})$ in Eq. (16) is the usual static XC kernel used in linear response time-dependent DFT [41–43].

For the mean-field Hartree potential, we have:

$$\Delta v_H(\mathbf{k}) = v_c(\mathbf{k}) \Delta n(\mathbf{k}), \quad v_c(\mathbf{k}) = \frac{4\pi}{k^2}. \tag{17}$$

It is convenient to define the *total* kernels:

$$\tilde{\mathcal{K}}_{\text{tot}}^{(2)}(\mathbf{k}) \equiv \tilde{\mathcal{K}}_s^{(2)}(\mathbf{k}) + v_c(\mathbf{k}) + \tilde{\mathcal{K}}_{xc}^{(2)}(\mathbf{k}), \tag{18}$$

$$\tilde{\mathcal{K}}_{\text{tot}}^{(3)}(\mathbf{k}|\mathbf{k}_1, \mathbf{k}_2) \equiv \tilde{\mathcal{K}}_s^{(3)}(\mathbf{k}|\mathbf{k}_1, \mathbf{k}_2) + \tilde{\mathcal{K}}_{xc}^{(3)}(\mathbf{k}|\mathbf{k}_1, \mathbf{k}_2), \tag{19}$$

$$\tilde{\mathcal{K}}_{\text{tot}}^{(4)}(\mathbf{k}|\mathbf{k}_1, \mathbf{k}_2, \mathbf{k}_3) \equiv \tilde{\mathcal{K}}_s^{(4)}(\mathbf{k}|\mathbf{k}_1, \mathbf{k}_2, \mathbf{k}_3) \tag{20}$$

$$+ \tilde{\mathcal{K}}_{xc}^{(4)}(\mathbf{k}|\mathbf{k}_1, \mathbf{k}_2, \mathbf{k}_3). \tag{21}$$

Inserting Eqs. (15), (16), and (17) into Eq. (7), and using notations for the total kernels, for each nonzero \mathbf{k} we finally get:

$$\begin{aligned}
&\tilde{\mathcal{K}}_{\text{tot}}^{(2)}(\mathbf{k}) \Delta n(\mathbf{k}) + \frac{1}{\Omega} \sum_{\substack{\mathbf{k}_1, \mathbf{k}_2 \\ \mathbf{k}=\mathbf{k}_1+\mathbf{k}_2}} \tilde{\mathcal{K}}_{\text{tot}}^{(3)}(\mathbf{k}|\mathbf{k}_1, \mathbf{k}_2) \Delta n(\mathbf{k}_1) \Delta n(\mathbf{k}_2) \\
&+ \frac{1}{\Omega^2} \sum_{\substack{\mathbf{k}_1, \mathbf{k}_2, \mathbf{k}_3 \\ \mathbf{k}=\mathbf{k}_1+\mathbf{k}_2+\mathbf{k}_3}} \tilde{\mathcal{K}}_{\text{tot}}^{(4)}(\mathbf{k}|\mathbf{k}_1, \mathbf{k}_2, \mathbf{k}_3) \Delta n(\mathbf{k}_1) \Delta n(\mathbf{k}_2) \Delta n(\mathbf{k}_3) \\
&+ \dots = -\Delta v_{\text{ext}}(\mathbf{k}).
\end{aligned} \tag{22}$$

One can rewrite Eq. (22) in a general compact form as

$$\tilde{\mathcal{K}}_{\text{tot}}^{(2)}(\mathbf{k}) \Delta n(\mathbf{k}) + \sum_{l=3}^{\infty} \left[\Omega^{2-l} \sum_{\substack{\mathbf{k}_1, \dots, \mathbf{k}_{l-1} \\ \mathbf{k}=\mathbf{k}_1+\dots+\mathbf{k}_{l-1}}} \tilde{\mathcal{K}}_{\text{tot}}^{(l)}(\mathbf{k}|\mathbf{k}_1, \dots, \mathbf{k}_{l-1}) \Delta n(\mathbf{k}_1) \dots \Delta n(\mathbf{k}_{l-1}) \right] = -\Delta v_{\text{ext}}(\mathbf{k}), \tag{23}$$

where

$$\tilde{\mathcal{K}}_{\text{tot}}^{(l)}(\mathbf{k}|\mathbf{k}_1, \dots, \mathbf{k}_{l-1}) \equiv \tilde{\mathcal{K}}_s^{(l)}(\mathbf{k}|\mathbf{k}_1, \dots, \mathbf{k}_{l-1}) + \tilde{\mathcal{K}}_{xc}^{(l)}(\mathbf{k}|\mathbf{k}_1, \dots, \mathbf{k}_{l-1}), \tag{24}$$

and $\tilde{\mathcal{K}}_{\text{tot}}^{(2)}(\mathbf{k})$ is defined in Eq. (18).

If we denote the left-hand side of Eq. (23) as $\Delta v_{\text{ind}}(\mathbf{k})$, we can express it as $\Delta v_{\text{ind}}(\mathbf{k}) = -\Delta v_{\text{ext}}(\mathbf{k})$, which means that the total induced potential exactly counteracts the external perturbation. Within linear density-response theory, this corresponds to omitting the sum on the left-hand side of Eq. (23).

For systems that are homogeneous on average, Eq. (23) can be utilized to analyze the density response of electrons to various types of external potentials, provided that the induced density perturbations can be expressed as a functional Taylor expansion around a homogeneous density value of the system. In the following, we will use Eq. (23) to derive the non-linear density response functions to a static harmonic external perturbation.

B. Task-Specific Formulation

Considering the harmonic perturbation in the form of

$$\Delta v_{\text{ext}}(\mathbf{r}) = 2A \cos(\mathbf{q} \cdot \mathbf{r}) = A e^{i\mathbf{q} \cdot \mathbf{r}} + A e^{-i\mathbf{q} \cdot \mathbf{r}}, \tag{25}$$

we now solve Eq. (23) order by order in A .

The discrete Fourier transform of $\Delta v_{\text{ext}}(\mathbf{r})$ reads:

$$\Delta v_{\text{ext}}(\mathbf{k}) = A \Omega [\delta_{\mathbf{k}, \mathbf{q}} + \delta_{\mathbf{k}, -\mathbf{q}}]. \tag{26}$$

External perturbation (25) induces a density perturbation represented by a harmonic expansion [15, 34]

$$\begin{aligned}
\Delta n(\mathbf{r}) &= 2\rho(\mathbf{q}) \cos(\mathbf{q} \cdot \mathbf{r}) \\
&+ 2\rho(2\mathbf{q}) \cos(2\mathbf{q} \cdot \mathbf{r}) + 2\rho(3\mathbf{q}) \cos(3\mathbf{q} \cdot \mathbf{r}) + \dots,
\end{aligned} \tag{27}$$

with the discrete Fourier transform:

$$\Delta n(\mathbf{k}) = \Omega \sum_m \rho(m\mathbf{q}) [\delta_{\mathbf{k}, m\mathbf{q}} + \delta_{\mathbf{k}, -m\mathbf{q}}], \tag{28}$$

where we consider solutions with $\rho(\mathbf{q}) = \rho^{(1)}(\mathbf{q}) + \rho^{(1,3)}(\mathbf{q}) = \mathcal{O}(A) + \mathcal{O}(A^3)$, $\rho(2\mathbf{q}) = \mathcal{O}(A^2)$, and $\rho(3\mathbf{q}) = \mathcal{O}(A^3)$. Factor two in Eq. (25) and Eq. (27) is a convention [8, 15, 26, 36].

The task is to use the DFT framework to find the density response functions defined as [8, 12, 14, 15, 34–36, 40]

$$\chi^{(1)}(\mathbf{q}) = \frac{\rho^{(1)}(\mathbf{q})}{A}, \quad \chi^{(1,3)}(\mathbf{q}) = \frac{\rho^{(1,3)}(\mathbf{q})}{A^3}, \quad (29)$$

and

$$\chi^{(2)}(\mathbf{q}) = \frac{\rho(2\mathbf{q})}{A^2}, \quad \chi^{(3)}(\mathbf{q}) = \frac{\rho(3\mathbf{q})}{A^3}, \quad (30)$$

where $\chi^{(1)}(\mathbf{q})$ is the linear density response function, $\chi^{(1,3)}(\mathbf{q})$ is the cubic density response function at the first harmonic, $\chi^{(2)}(\mathbf{q})$ is the quadratic density response function at the second harmonic, and $\chi^{(3)}(\mathbf{q})$ is the cubic density response function at the third harmonic.

C. Linear response at $\mathbf{k} = \mathbf{q}$

As an introductory exercise, we first recover known results for the linear density response function. For $\mathbf{k} = \mathbf{q}$, at first order in A , we have $\Delta n(\mathbf{q}) \simeq \Delta n^{(1)}(\mathbf{q}) = \rho^{(1)}(\mathbf{q})\Omega$ (the term with $m = 1$ in Eq. (28)). In this case, following (23), we write:

$$\tilde{\mathcal{K}}_{\text{tot}}^{(2)}(\mathbf{q}) \Delta n^{(1)}(\mathbf{q}) = -\Delta v_{\text{ext}}(\mathbf{q}), \quad (31)$$

from which, taking into account that $\Delta v_{\text{ext}}(\mathbf{q}) = A\Omega$ and $\Delta n^{(1)}(\mathbf{q}) = \rho^{(1)}(\mathbf{q})\Omega$, we find a known result for the linear density response function:

$$\chi^{(1)}(\mathbf{q}) \equiv \frac{\delta n^{(1)}(\mathbf{q})}{\delta v_{\text{ext}}(\mathbf{q})} = \frac{\rho^{(1)}(\mathbf{q})}{A} \quad (32)$$

$$= -\frac{1}{\tilde{\mathcal{K}}_{\text{tot}}^{(2)}(\mathbf{q})} = -\frac{1}{\tilde{\mathcal{K}}_s^{(2)}(\mathbf{q}) + v_c(\mathbf{q}) + \tilde{\mathcal{K}}_{\text{xc}}^{(2)}(\mathbf{q})}. \quad (33)$$

By symmetry $\delta n^{(1)}(-\mathbf{q}) = \delta n^{(1)}(\mathbf{q})$ and $\chi^{(1)}(-\mathbf{q}) = \chi^{(1)}(\mathbf{q})$.

It is a convention to denote

$$\chi_0^{(1)}(\mathbf{q}) = -\frac{1}{\tilde{\mathcal{K}}_s^{(2)}(\mathbf{q})}, \quad (34)$$

with $\chi_0(\mathbf{q})$ being referred to as the non-interacting density response. This function $\chi_0(\mathbf{q})$ is given by the Lindhard function for the UEG and by the KS-response function in DFT [40, 44].

Using Eq. (34) in Eq. (33), we arrive at a standard form of the linear density response function from the theory of quantum liquids [45]:

$$\chi^{(1)}(\mathbf{q}) = \frac{\chi_0^{(1)}(\mathbf{q})}{1 - (v_c(\mathbf{q}) + \tilde{\mathcal{K}}_{\text{xc}}^{(2)}(\mathbf{q}))\chi_0^{(1)}(\mathbf{q})}. \quad (35)$$

The random phase approximation (RPA) follows from Eq. (35) if we neglect XC contributions by setting $\tilde{\mathcal{K}}_{\text{xc}}^{(2)}(\mathbf{q}) \equiv 0$ (denoted as $\chi_{\text{RPA}}^{(1)}(\mathbf{q})$).

D. Quadratic response at second harmonic $\mathbf{k} = 2\mathbf{q}$

Next, we compute the response at $2\mathbf{q}$, which emerges to be $\mathcal{O}(A^2)$. For that, we set $\mathbf{k} = 2\mathbf{q}$ in Eq. (23), where now $\Delta v_{\text{ext}}(2\mathbf{q}) = 0$ because there is no direct external perturbation at $2\mathbf{q}$. In Eq. (23), we consider terms up to $\mathcal{O}(A^2)$. Taking into account momentum conservation, we set $\mathbf{k}_1 = \mathbf{q}$ and $\mathbf{k}_2 = \mathbf{q}$, resulting from the condition $2\mathbf{q} = \mathbf{k}_1 + \mathbf{k}_2$. Other combinations would yield higher-order terms in A . Additionally, we exclude terms with $\mathbf{k}_1 = 0$ or $\mathbf{k}_2 = 0$ as they cancel out due to the conservation of the number of particles. Therefore, Eq. (23) gives us the quadratic response of the form:

$$\tilde{\mathcal{K}}_{\text{tot}}^{(2)}(2\mathbf{q}) \Delta n(2\mathbf{q}) + \frac{1}{\Omega} \tilde{\mathcal{K}}_{\text{tot}}^{(3)}(2\mathbf{q}|\mathbf{q}, \mathbf{q}) \Delta n(\mathbf{q}) \Delta n(\mathbf{q}) = 0. \quad (36)$$

Eq. (36) then leads to:

$$\Delta n(2\mathbf{q}) = -\frac{\tilde{\mathcal{K}}_{\text{tot}}^{(3)}(2\mathbf{q}|\mathbf{q}, \mathbf{q})}{\tilde{\mathcal{K}}_{\text{tot}}^{(2)}(2\mathbf{q})} \frac{(\Delta n(\mathbf{q}))^2}{\Omega}. \quad (37)$$

From Eq. (37), by using $\Delta n(\mathbf{q}) \simeq \Delta n^{(1)}(\mathbf{q})$, along with Eqs. (32) and (33), and taking into account that $\Delta n(2\mathbf{q}) = \Omega \rho(2\mathbf{q})$ and $\Delta v_{\text{ext}}(\mathbf{q}) = A\Omega$, we derive

$$\rho(2\mathbf{q}) = \tilde{\mathcal{K}}_{\text{tot}}^{(3)}(2\mathbf{q}|\mathbf{q}, \mathbf{q}) \chi^{(1)}(2\mathbf{q}) [\chi^{(1)}(\mathbf{q})]^2 A^2, \quad (38)$$

from which we find:

$$\chi^{(2)}(\mathbf{q}) \equiv \frac{\rho(2\mathbf{q})}{A^2} = \tilde{\mathcal{K}}_{\text{tot}}^{(3)}(2\mathbf{q}|\mathbf{q}, \mathbf{q}) \chi^{(1)}(2\mathbf{q}) [\chi^{(1)}(\mathbf{q})]^2. \quad (39)$$

Solution (39) for the quadratic response is applicable for any disordered material for which averaging over ion configurations (snapshots) leads to a homogeneous electron density. Let us analyze Eq. (39) in the limit of the UEG and show the connection with the results from previous works.

Eq. (36) allows us to understand the origin of the quadratic density response at the second harmonic. For that we rewrite Eq. (36) as

$$\tilde{\mathcal{K}}_{\text{tot}}^{(2)}(2\mathbf{q}) \Delta n(2\mathbf{q}) = v_{\text{ind}}^{(2)}(2\mathbf{q}), \quad (40)$$

where

$$v_{\text{ind}}^{(2)}(2\mathbf{q}) = \frac{1}{\Omega} \tilde{\mathcal{K}}_{\text{tot}}^{(3)}(2\mathbf{q}|\mathbf{q}, \mathbf{q}) \Delta n(\mathbf{q}) \Delta n(\mathbf{q}). \quad (41)$$

From Eqs. (40) and (41), we see that the quadratic density response at the second harmonic is the linear reaction to the second-order field $v_{\text{ind}}^{(2)}(2\mathbf{q})$ from the expansion of the perturbation of the total induced potential.

Considering the non-interacting UEG with $\tilde{\mathcal{K}}_{\text{tot}}^{(3)} \rightarrow \tilde{\mathcal{K}}_s^{(3)}$, $\chi^{(2)} \rightarrow \chi_0^{(2)}$, and $\chi^{(1)} \rightarrow \chi_0$, from Eq. (39) we derive:

$$\tilde{\mathcal{K}}_s^{(3)}(2\mathbf{q}|\mathbf{q}, \mathbf{q}) = \frac{\chi_0^{(2)}(\mathbf{q})}{\chi_0^{(1)}(2\mathbf{q}) [\chi_0^{(1)}(\mathbf{q})]^2}, \quad (42)$$

where $\chi_0^{(2)}(\mathbf{q})$ was shown to be expressed in terms of the ideal linear density response function $\chi_0^{(1)}(\mathbf{q})$ by Mikhailov [35]:

$$\chi_0^{(2)}(\mathbf{q}) = \frac{2}{q^2} \left(\chi_0^{(1)}(2\mathbf{q}) - \chi_0^{(1)}(\mathbf{q}) \right). \quad (43)$$

$$\chi^{(2)}(\mathbf{q}) = \left[\frac{\chi_0^{(2)}(\mathbf{q})}{\chi_0^{(1)}(2\mathbf{q}) [\chi_0^{(1)}(\mathbf{q})]^2} + \tilde{\mathcal{K}}_{\text{xc}}^{(3)}(2\mathbf{q}|\mathbf{q}, \mathbf{q}) \right] \chi^{(1)}(2\mathbf{q}) [\chi^{(1)}(\mathbf{q})]^2, \quad (44)$$

from which one can see that full inclusion of the XC effects in $\chi^{(2)}(\mathbf{q})$ of the UEG requires $\tilde{\mathcal{K}}_{\text{xc}}^{(3)}(2\mathbf{q}|\mathbf{q}, \mathbf{q})$, i.e., the third-order functional derivative of the XC functional [46].

If we neglect the contribution $\tilde{\mathcal{K}}_{\text{xc}}^{(3)}(2\mathbf{q}|\mathbf{q}, \mathbf{q})$, Eq. (44) reproduces the result derived in Ref. [15]:

$$\chi^{(2)}(\mathbf{q}) = \chi_0^{(2)}(\mathbf{q}) \left[1 - v_c(\mathbf{q}) [1 - G(\mathbf{q})] \chi_0^{(1)}(\mathbf{q}) \right]^{-2} \times \left[1 - v_c(2\mathbf{q}) [1 - G(2\mathbf{q})] \chi_0^{(1)}(2\mathbf{q}) \right]^{-1}, \quad (45)$$

where we applied Eq. (35) and introduced the local field correction $G(\mathbf{q}) = -\tilde{\mathcal{K}}_{\text{xc}}^{(2)}(\mathbf{q})/v_c(\mathbf{q})$, which is frequently used in the theory of the UEG and quantum liquids [45, 47–49], instead of the kernel $\tilde{\mathcal{K}}_{\text{xc}}^{(2)}(\mathbf{q})$. Thus, approximation (45) neglects $\tilde{\mathcal{K}}_{\text{xc}}^{(3)}(2\mathbf{q}|\mathbf{q}, \mathbf{q})$.

Within RPA, i.e., setting $\tilde{\mathcal{K}}_{\text{xc}}^{(3)}(2\mathbf{q}|\mathbf{q}, \mathbf{q}) = 0$ and $\tilde{\mathcal{K}}_{\text{xc}}^{(2)}(\mathbf{q}) = 0$, we find from Eq. (44):

$$\chi_{\text{RPA}}^{(2)}(\mathbf{q}) = \chi_0^{(2)}(\mathbf{q}) \left[1 - v_c(\mathbf{q}) \chi_0^{(1)}(\mathbf{q}) \right]^{-2} \times \left[1 - v_c(2\mathbf{q}) \chi_0^{(1)}(2\mathbf{q}) \right]^{-1}, \quad (46)$$

which agrees with the result by derived using the method of Green's function (e.g., see Refs. [3, 50, 51]).

One can express $\tilde{\mathcal{K}}_{\text{xc}}^{(3)}(2\mathbf{q}|\mathbf{q}, \mathbf{q})$ in terms of the linear and quadratic density response functions:

$$\tilde{\mathcal{K}}_{\text{xc}}^{(3)}(2\mathbf{q}|\mathbf{q}, \mathbf{q}) = \frac{\chi^{(2)}(\mathbf{q})}{\chi^{(1)}(2\mathbf{q}) [\chi^{(1)}(\mathbf{q})]^2} - \frac{\chi_0^{(2)}(\mathbf{q})}{\chi_0^{(1)}(2\mathbf{q}) [\chi_0^{(1)}(\mathbf{q})]^2}. \quad (47)$$

Eq. (47) allows one to compute $\tilde{\mathcal{K}}_{\text{xc}}^{(3)}(2\mathbf{q}|\mathbf{q}, \mathbf{q})$ without performing third order functional derivatives by using the data for $\chi^{(2)}(\mathbf{q})$, $\chi_0^{(2)}(\mathbf{q})$, $\chi_0^{(1)}(\mathbf{q})$, and $\chi_0^{(1)}(\mathbf{q})$ from the simulation of electrons perturbed by field (25). Such an approach was extensively used to compute the static XC kernel $\tilde{\mathcal{K}}_{\text{xc}}^{(2)}(\mathbf{q})$ for the UEG and warm dense hydrogen to analyze various XC functionals often used DFT [42, 43, 52–56]. Similarly, Eq. (47) can be used to analyze XC functionals on the level of the third-order functional derivatives. For example, exact quantum Monte

Now, for $\chi^{(2)}(\mathbf{q})$ of the UEG, we find:

Carlo data for $\tilde{\mathcal{K}}_{\text{xc}}^{(3)}(2\mathbf{q}|\mathbf{q}, \mathbf{q})$ of the UEG can be used as an additional constraint for the development of new XC functionals with improved consistency.

E. Cubic response at the first harmonic $\mathbf{k} = \mathbf{q}$

Next, we examine the cubic response at the first harmonic, denoted as $\chi^{(1,3)}(\mathbf{q})$ and defined in Eq. (29). Previous attempts to find an analytic solution for $\chi^{(1,3)}(\mathbf{q})$, utilizing the method of Green's functions [3] and quantum-kinetic theory [12], were unsuccessful, leading to a conspicuous absence of theoretical results for this case. Here, we conclusively overcome this problem using the present DFT framework.

First, in addition to the linear response term, we include the $\mathcal{O}(A^3)$ term in $\Delta n(\mathbf{k} = \mathbf{q})$:

$$\Delta n(\mathbf{q}) = \Delta n^{(1)}(\mathbf{q}) + \Delta n^{(3)}(\mathbf{q}), \quad (48)$$

where $\Delta n^{(1)}(\mathbf{q}) = \chi^{(1)}(\mathbf{q}) A \Omega$, and $\Delta n^{(3)}(\mathbf{q}) = \chi^{(1,3)}(\mathbf{q}) A^3 \Omega$ is to be found.

We set $\mathbf{k} = \mathbf{q}$ in Eq. (23), and expand to $\mathcal{O}(A^3)$. The left-hand side has three pieces:

1. For the linear term, we have:

$$\tilde{\mathcal{K}}_{\text{tot}}^{(2)}(\mathbf{q}) \Delta n(\mathbf{q}) = \tilde{\mathcal{K}}_{\text{tot}}^{(2)}(\mathbf{q}) [\Delta n^{(1)}(\mathbf{q}) + \Delta n^{(3)}(\mathbf{q})], \quad (49)$$

which, at $\mathcal{O}(A)$, matches $-\Delta v_{\text{ext}}(\mathbf{q})$ on the r.h.s. of Eq. (23), and has already been considered. Therefore, only the piece $\tilde{\mathcal{K}}_{\text{tot}}^{(2)}(\mathbf{q}) \Delta n^{(3)}(\mathbf{q}) \sim \mathcal{O}(A^3)$ remains.

2. In the quadratic term

$$\frac{1}{\Omega} \sum_{\substack{\mathbf{k}_1, \mathbf{k}_2 \\ \mathbf{q} = \mathbf{k}_1 + \mathbf{k}_2}} \tilde{\mathcal{K}}_{\text{tot}}^{(3)}(\mathbf{q}|\mathbf{k}_1, \mathbf{k}_2) \Delta n(\mathbf{k}_1) \Delta n(\mathbf{k}_2), \quad (50)$$

to get $\mathcal{O}(A^3)$, we must use one mode of order A^2 and one of order A . The only such combination of $(\mathbf{k}_1, \mathbf{k}_2)$ that sums to \mathbf{q} at this order is $(2\mathbf{q}, -\mathbf{q})$ and $(-\mathbf{q}, 2\mathbf{q})$. Both give the same contribution by symmetry, yielding

$$\frac{2}{\Omega} \tilde{\mathcal{K}}_{\text{tot}}^{(3)}(\mathbf{q}|2\mathbf{q}, -\mathbf{q}) \Delta n(2\mathbf{q}) \Delta n(-\mathbf{q}). \quad (51)$$

3. In the cubic term, we consider

$$\frac{1}{\Omega^2} \sum_{\substack{\mathbf{k}_1, \mathbf{k}_2, \mathbf{k}_3 \\ \mathbf{q} = \mathbf{k}_1 + \mathbf{k}_2 + \mathbf{k}_3}} \tilde{\mathcal{K}}_{\text{tot}}^{(4)}(\mathbf{q}|\mathbf{k}_1, \mathbf{k}_2, \mathbf{k}_3) \Delta n(\mathbf{k}_1) \Delta n(\mathbf{k}_2) \Delta n(\mathbf{k}_3). \quad (52)$$

with three fundamental modes $\Delta n \propto A$. The only triples $(\mathbf{k}_1, \mathbf{k}_2, \mathbf{k}_3)$ that sum to \mathbf{q} are permutations of $(\mathbf{q}, \mathbf{q}, -\mathbf{q})$. There are three such permutations. Thus, this cubic part becomes

$$\frac{3}{\Omega^2} \tilde{\mathcal{K}}_{\text{tot}}^{(4)}(\mathbf{q}|\mathbf{q}, \mathbf{q}, -\mathbf{q}) \Delta n(\mathbf{q}) \Delta n(\mathbf{q}) \Delta n(-\mathbf{q}). \quad (53)$$

Putting all of this together, the $\mathbf{k} = \mathbf{q}$ component of Eq. (23) at $\mathcal{O}(A^3)$ becomes

$$\begin{aligned} & \tilde{\mathcal{K}}_{\text{tot}}^{(2)}(\mathbf{q}) \Delta n^{(3)}(\mathbf{q}) + \frac{2}{\Omega} \tilde{\mathcal{K}}_{\text{tot}}^{(3)}(\mathbf{q}|\mathbf{2q}, -\mathbf{q}) \Delta n(\mathbf{2q}) \Delta n(-\mathbf{q}) \\ & + \frac{3}{\Omega^2} \tilde{\mathcal{K}}_{\text{tot}}^{(4)}(\mathbf{q}|\mathbf{q}, \mathbf{q}, -\mathbf{q}) [\Delta n(\mathbf{q})]^2 \Delta n(-\mathbf{q}) = 0. \end{aligned} \quad (54)$$

Solving Eq. (54) for $\Delta n^{(3)}(\mathbf{q})$, one derives:

$$\begin{aligned} \Delta n^{(3)}(\mathbf{q}) = & -\frac{1}{\tilde{\mathcal{K}}_{\text{tot}}^{(2)}(\mathbf{q})} \left[\frac{2}{\Omega} \tilde{\mathcal{K}}_{\text{tot}}^{(3)}(\mathbf{q}|\mathbf{2q}, -\mathbf{q}) \Delta n(\mathbf{2q}) \Delta n(-\mathbf{q}) \right. \\ & \left. + \frac{3}{\Omega^2} \tilde{\mathcal{K}}_{\text{tot}}^{(4)}(\mathbf{q}|\mathbf{q}, \mathbf{q}, -\mathbf{q}) [\Delta n(\mathbf{q})]^2 \Delta n(-\mathbf{q}) \right], \end{aligned} \quad (55)$$

where we substitute $\Delta n(\mathbf{q}) = \chi^{(1)}(\mathbf{q}) A \Omega$, $\Delta n(-\mathbf{q}) = \chi^{(1)}(\mathbf{q}) A \Omega$, $\Delta n(\mathbf{2q}) = \Omega \rho(\mathbf{2q}) = \Omega \chi^{(2)}(\mathbf{q}) A^2$, and Eq. (38), to write for the first product:

$$\begin{aligned} \Delta n(\mathbf{2q}) \Delta n(-\mathbf{q}) &= \rho(\mathbf{2q}) \chi^{(1)}(\mathbf{q}) A \Omega^2 \\ &= \chi^{(2)}(\mathbf{q}) \chi^{(1)}(\mathbf{q}) A^3 \Omega^2, \end{aligned} \quad (56)$$

$$= \tilde{\mathcal{K}}_{\text{tot}}^{(3)}(\mathbf{2q}|\mathbf{q}, \mathbf{q}) \chi^{(1)}(\mathbf{2q}) [\chi^{(1)}(\mathbf{q})]^3 A^3 \Omega^2, \quad (57)$$

and for the second product:

$$[\Delta n(\mathbf{q})]^2 \Delta n(-\mathbf{q}) = [\chi^{(1)}(\mathbf{q})]^3 A^3 \Omega^3. \quad (58)$$

Substituting Eqs. (57) and (58) into Eq. (55), and taking into account that $\chi^{(1)}(\mathbf{q}) = -1/\tilde{\mathcal{K}}_{\text{tot}}^{(2)}(\mathbf{q})$, we obtain:

$$\begin{aligned} \Delta n^{(3)}(\mathbf{q}) = & A^3 \Omega [\chi^{(1)}(\mathbf{q})]^4 \left[3 \tilde{\mathcal{K}}_{\text{tot}}^{(4)}(\mathbf{q}|\mathbf{q}, \mathbf{q}, -\mathbf{q}) \right. \\ & \left. + 2 \tilde{\mathcal{K}}_{\text{tot}}^{(3)}(\mathbf{q}|\mathbf{2q}, -\mathbf{q}) \tilde{\mathcal{K}}_{\text{tot}}^{(3)}(\mathbf{2q}|\mathbf{q}, \mathbf{q}) \chi^{(1)}(\mathbf{2q}) \right], \end{aligned} \quad (59)$$

from which, using $\Delta n^{(3)}(\mathbf{q}) = \rho^{(1,3)}(\mathbf{q}) \Omega$, we finally get the cubic response at the first harmonic:

$$\begin{aligned} \chi^{(1,3)}(\mathbf{q}) &\equiv \frac{\rho^{(1,3)}(\mathbf{q})}{A^3} \\ &= [\chi^{(1)}(\mathbf{q})]^4 \left[3 \tilde{\mathcal{K}}_{\text{tot}}^{(4)}(\mathbf{q}|\mathbf{q}, \mathbf{q}, -\mathbf{q}) \right. \\ &\quad \left. + 2 \tilde{\mathcal{K}}_{\text{tot}}^{(3)}(\mathbf{q}|\mathbf{2q}, -\mathbf{q}) \tilde{\mathcal{K}}_{\text{tot}}^{(3)}(\mathbf{2q}|\mathbf{q}, \mathbf{q}) \chi^{(1)}(\mathbf{2q}) \right], \end{aligned} \quad (60)$$

which is our general solution for $\chi^{(1,3)}(\mathbf{q})$.

To understand the origin of the cubic response at first harmonic, one can rewrite Eq. (60) as

$$\rho^{(1,3)}(\mathbf{q}) = \chi^{(1)}(\mathbf{q}) \left([A_{\text{ind}}(\mathbf{q}, \mathbf{q}, -\mathbf{q})]^3 + [A_{\text{ind}}(\mathbf{2q}, -\mathbf{q})]^3 \right) \quad (61)$$

where

$$[A_{\text{ind}}(\mathbf{q}, \mathbf{q}, -\mathbf{q})]^3 = 3 \tilde{\mathcal{K}}_{\text{tot}}^{(4)}(\mathbf{q}|\mathbf{q}, \mathbf{q}, -\mathbf{q}) [\chi^{(1)}(\mathbf{q})]^2 \chi^{(1)}(-\mathbf{q}) A^3. \quad (62)$$

and

$$[A_{\text{ind}}(\mathbf{2q}, -\mathbf{q})]^3 = 2 \tilde{\mathcal{K}}_{\text{tot}}^{(3)}(\mathbf{q}|\mathbf{2q}, -\mathbf{q}) \chi^{(2)}(\mathbf{q}) \chi^{(1)}(-\mathbf{q}) A^3. \quad (63)$$

Physically, Eq. (62) tells us that the external perturbation at wavevector $\mathbf{k} = \mathbf{q}$ induces three $\mathcal{O}(A)$ -order density perturbations at modes $(\mathbf{q}, \mathbf{q}, -\mathbf{q})$ that couple with each other to generate a $\mathcal{O}(A^3)$ -order response at the first harmonic (with the coupling being defined by the kernel $\tilde{\mathcal{K}}_{\text{tot}}^{(4)}(\mathbf{q}|\mathbf{q}, \mathbf{q}, -\mathbf{q})$). Eq. (63) tells us that the external perturbation at wavevector $\mathbf{k} = \mathbf{q}$ also induces a $\mathcal{O}(A^2)$ -order density perturbation at $\mathbf{2q}$ that couples with the $\mathcal{O}(A)$ -order density perturbation at $-\mathbf{q}$ (with the coupling being given by the kernel $\tilde{\mathcal{K}}_{\text{tot}}^{(3)}(\mathbf{q}|\mathbf{2q}, -\mathbf{q})$) that generates the $\mathcal{O}(A^3)$ order response at the first harmonic. Thus, density perturbation (61) is the result of the mode coupling of fields generated by induced densities at the second and first harmonics.

Our new result (60) provides a solution in terms of the functional derivatives of $F_s[n]$ and $F_{\text{xc}}[n]$. Although the exact forms of both $F_s[n]$ and $F_{\text{xc}}[n]$ are unknown, there are a number of well-tested approximations for $F_s[n]$ and $F_{\text{xc}}[n]$ (e.g., for finite temperatures, see Refs. [57, 58] and, for the ground state, see Refs. [59, 60]). In addition, the non-interacting free energy is computed exactly in KS-DFT, allowing for the computation of the density response functions using the direct perturbation approach without relying on approximations for $F_s[n]$ [8, 43]. Furthermore, for the UEG, at small wavenumbers $\mathbf{q} \rightarrow 0$, the exact solution for $F_s[n]$ is given by the Thomas-Fermi solution for the free energy $F_{\text{TF}}[n]$ [61, 62].

Let us now analyze $\chi^{(1,3)}(\mathbf{q})$ in the limit of the UEG. For that, we first denote

$$\begin{aligned} \Gamma_{\text{tot}}^{(1,3)}(\mathbf{q}) &= 3 \tilde{\mathcal{K}}_{\text{tot}}^{(4)}(\mathbf{q}|\mathbf{q}, \mathbf{q}, -\mathbf{q}) \\ &\quad + 2 \tilde{\mathcal{K}}_{\text{tot}}^{(3)}(\mathbf{q}|\mathbf{2q}, -\mathbf{q}) \tilde{\mathcal{K}}_{\text{tot}}^{(3)}(\mathbf{2q}|\mathbf{q}, \mathbf{q}) \chi^{(1)}(\mathbf{2q}). \end{aligned} \quad (64)$$

In the case of the ideal UEG, neglecting XC terms, we have

$$\begin{aligned} \Gamma_s^{(1,3)}(\mathbf{q}) &= 3 \tilde{\mathcal{K}}_s^{(4)}(\mathbf{q}|\mathbf{q}, \mathbf{q}, -\mathbf{q}) \\ &\quad + 2 \tilde{\mathcal{K}}_s^{(3)}(\mathbf{q}|\mathbf{2q}, -\mathbf{q}) \tilde{\mathcal{K}}_s^{(3)}(\mathbf{2q}|\mathbf{q}, \mathbf{q}) \chi_0^{(1)}(\mathbf{2q}). \end{aligned} \quad (65)$$

The exact $\mathbf{q} \rightarrow 0$ limit of $F_s[n]$ is given by the TF non-interacting free energy functional $F_{\text{TF}}[n]$, for which the Fourier transforms of the functional derivatives do not depend on \mathbf{q} . In addition, we recall that the $\mathbf{q} \rightarrow 0$ limit of $\chi_0^{(1)}(\mathbf{q})$ is a finite number. Thus, we can write:

$$\Gamma_s^{(1,3)}(\mathbf{q} \rightarrow 0) = \Gamma_{\text{TF}}^{(1,3)}, \quad (66)$$

and find

$$\chi_0^{(1,3)}(\mathbf{q} \rightarrow 0) = \left[\chi_0^{(1)}(\mathbf{q} \rightarrow 0) \right]^4 \times \Gamma_{\text{TF}}^{(1,3)}. \quad (67)$$

The reduced kernels of the TF model for calculating the long wavelength limit of the considered non-linear response functions are provided in Appendix A.

As an approximation for $\chi_0^{(1,3)}(\mathbf{q})$, one can use the TF approximation for $\tilde{\mathcal{K}}_s^{(3)}$ in Eq. (60), and find:

$$\chi_0^{(1,3)}(\mathbf{q}) \approx \left[\chi_0^{(1)}(\mathbf{q}) \right]^4 \left[3 \tilde{\mathcal{K}}_{\text{TF}}^{(4)} + 2 \left[\tilde{\mathcal{K}}_{\text{TF}}^{(3)} \right]^2 \chi_0^{(1)}(2\mathbf{q}) \right]. \quad (68)$$

This approximation can be expected to give an adequate q dependence of $\chi_0^{(1,3)}(\mathbf{q})$ at small wavenumbers. We test the quality of this approximation by comparing it with the results of exact numerical calculations for the UEG.

F. Cubic response at the third harmonic $\mathbf{k} = 3\mathbf{q}$

Lastly, we consider the $\mathcal{O}(A^3)$ terms at $\mathbf{k} = 3\mathbf{q}$ in Eq. (23):

$$\begin{aligned} K_2^{\text{tot}}(3\mathbf{q}) \Delta n(3\mathbf{q}) + \frac{1}{\Omega} \tilde{\mathcal{K}}_{\text{tot}}^{(3)}(3\mathbf{q}|2\mathbf{q}, \mathbf{q}) \Delta n(2\mathbf{q}) \Delta n(\mathbf{q}) \\ + \frac{1}{\Omega^2} \tilde{\mathcal{K}}_{\text{tot}}^{(4)}(3\mathbf{q}|\mathbf{q}, \mathbf{q}, \mathbf{q}) \Delta n(\mathbf{q})^3 = 0, \end{aligned} \quad (69)$$

where we took into account that $\Delta v_{\text{ext}}(3\mathbf{q}) = 0$, a $\tilde{\mathcal{K}}_{\text{tot}}^{(3)}$ term mixing $\Delta n(2\mathbf{q})$ (order A^2) and $\Delta n(\mathbf{q})$ (order A), because $2\mathbf{q} + \mathbf{q} = 3\mathbf{q}$, and a $\tilde{\mathcal{K}}_{\text{tot}}^{(4)}$ term mixing $\Delta n(\mathbf{q})\Delta n(\mathbf{q})\Delta n(\mathbf{q})$, because $\mathbf{q} + \mathbf{q} + \mathbf{q} = 3\mathbf{q}$.

Solving Eq. (69) for $\Delta n(3\mathbf{q})$, one finds:

$$\begin{aligned} \Delta n(3\mathbf{q}) = - \frac{1}{K_2^{\text{tot}}(3\mathbf{q})} \left[\frac{1}{\Omega} \tilde{\mathcal{K}}_{\text{tot}}^{(3)}(3\mathbf{q}|2\mathbf{q}, \mathbf{q}) \Delta n(2\mathbf{q}) \Delta n(\mathbf{q}) \right. \\ \left. + \frac{1}{\Omega^2} \tilde{\mathcal{K}}_{\text{tot}}^{(4)}(3\mathbf{q}|\mathbf{q}, \mathbf{q}, \mathbf{q}) [\Delta n(\mathbf{q})]^3 \right], \end{aligned} \quad (70)$$

which shows the contribution originated from the coupling of three $\mathcal{O}(A)$ -order density perturbations at modes $(\mathbf{q}, \mathbf{q}, \mathbf{q})$ and another contribution from the coupling of $\mathcal{O}(A^2)$ -order density perturbation at $2\mathbf{q}$ with $\mathcal{O}(A)$ -order density perturbation at \mathbf{q} .

Substituting $\Delta n(\mathbf{q}) \simeq \Delta n^{(1)}(\mathbf{q}) = \chi^{(1)}(\mathbf{q})A\Omega$, $\Delta n(2\mathbf{q}) = \Omega\rho(2\mathbf{q})$, into Eq. (70), taking into account Eq. (38) and that $\chi^{(1)}(3\mathbf{q}) = -1/\tilde{\mathcal{K}}_{\text{tot}}^{(2)}(3\mathbf{q})$, we derive:

$$\rho(3\mathbf{q}) = \chi^{(1)}(3\mathbf{q}) \left[\chi^{(1)}(\mathbf{q}) \right]^3 \Gamma_{\text{tot}}^{(3)}(\mathbf{q}) A^3, \quad (71)$$

where

$$\begin{aligned} \Gamma_{\text{tot}}^{(3)}(\mathbf{q}) = \left[\tilde{\mathcal{K}}_{\text{tot}}^{(3)}(3\mathbf{q}|2\mathbf{q}, \mathbf{q}) \tilde{\mathcal{K}}_{\text{tot}}^{(3)}(2\mathbf{q}|\mathbf{q}, \mathbf{q}) \chi^{(1)}(2\mathbf{q}) \right. \\ \left. + \tilde{\mathcal{K}}_{\text{tot}}^{(4)}(3\mathbf{q}|\mathbf{q}, \mathbf{q}, \mathbf{q}) \right]. \end{aligned} \quad (72)$$

Finally, for the cubic response at third harmonic, Eq. (70) then gives:

$$\chi^{(3)}(\mathbf{q}) \equiv \frac{\rho(3\mathbf{q})}{A^3} = \chi^{(1)}(3\mathbf{q}) \left[\chi^{(1)}(\mathbf{q}) \right]^3 \Gamma_{\text{tot}}^{(3)}(\mathbf{q}). \quad (73)$$

Eq. (73) is a general solution for the cubic response function at the third harmonic of electrons in homogeneous systems. Let us now consider the UEG limit.

For the ideal UEG, Mikhailov expressed the ideal cubic response function at the third harmonic $\chi_0^{(3)}(\mathbf{q})$ in terms of $\chi_0^{(1)}(\mathbf{q})$ [34, 35]:

$$\chi_0^{(3)}(\mathbf{q}) = \frac{3\chi_0^{(1)}(3\mathbf{q}) - 8\chi_0^{(1)}(2\mathbf{q}) + 5\chi_0^{(1)}(\mathbf{q})}{3\mathbf{q}^4}. \quad (74)$$

For the ideal UEG, from Eq. (73) and Eq. (74), we find:

$$\frac{\chi_0^{(3)}(\mathbf{q})}{\chi_0^{(1)}(3\mathbf{q}) \left[\chi_0^{(1)}(\mathbf{q}) \right]^3} = \Gamma_s^{(3)}(\mathbf{q}), \quad (75)$$

where $\Gamma_s^{(3)}(\mathbf{q})$ follows from $\Gamma_{\text{tot}}^{(3)}(\mathbf{q})$ if we neglect the Hartree and XC terms:

$$\begin{aligned} \Gamma_s^{(3)}(\mathbf{q}) = \tilde{\mathcal{K}}_s^{(3)}(3\mathbf{q}|2\mathbf{q}, \mathbf{q}) \tilde{\mathcal{K}}_s^{(3)}(2\mathbf{q}|\mathbf{q}, \mathbf{q}) \chi_0^{(1)}(2\mathbf{q}) \\ + \tilde{\mathcal{K}}_s^{(4)}(3\mathbf{q}|\mathbf{q}, \mathbf{q}, \mathbf{q}). \end{aligned} \quad (76)$$

Now, considering the density response of the interacting electrons with approximation $\Gamma_{\text{tot}}^{(3)}(\mathbf{q}) \simeq \Gamma_s^{(3)}(\mathbf{q})$ in Eq. (73), using Eq. (75) and Eq. (35), we deduce the result

$$\begin{aligned} \chi^{(3)}(\mathbf{q}) = \chi_0^{(3)}(\mathbf{q}) \left[1 - v(\mathbf{q}) [1 - G(\mathbf{q})] \chi_0^{(1)}(\mathbf{q}) \right]^{-3} \\ \times \left[1 - v(3\mathbf{q}) [1 - G(3\mathbf{q})] \chi_0^{(1)}(3\mathbf{q}) \right]^{-1}, \end{aligned} \quad (77)$$

where we used $G(\mathbf{q}) = -\tilde{\mathcal{K}}_{\text{xc}}^{(2)}(\mathbf{q})/v_c(\mathbf{q})$.

In the RPA, setting $\tilde{\mathcal{K}}_{\text{xc}}^{(3)}(3\mathbf{q}, 2\mathbf{q}, \mathbf{q}) = 0$, $\tilde{\mathcal{K}}_{\text{xc}}^{(3)}(2\mathbf{q}|\mathbf{q}, \mathbf{q}) = 0$, $\tilde{\mathcal{K}}_{\text{xc}}^{(4)}(3\mathbf{q}|\mathbf{q}, \mathbf{q}, \mathbf{q}) = 0$, and $\tilde{\mathcal{K}}_{\text{xc}}^{(2)}(\mathbf{q}) = 0$, we find from Eq. (73):

$$\chi_{\text{RPA}}^{(3)}(\mathbf{q}) = \chi_{\text{RPA}}^{(1)}(3\mathbf{q}) \left[\chi_{\text{RPA}}^{(1)}(\mathbf{q}) \right]^3 \Gamma_{\text{RPA}}^{(3)}(\mathbf{q}). \quad (78)$$

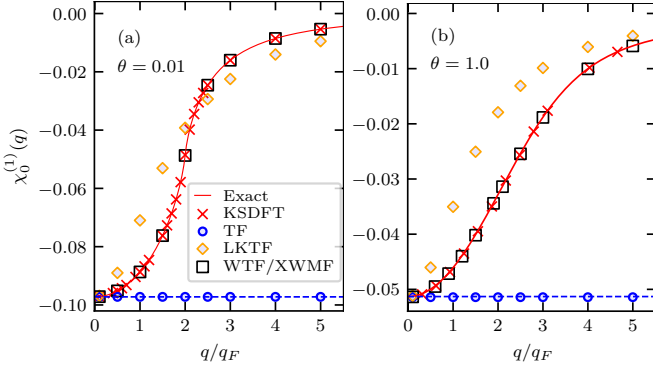


FIG. 1. Linear static density response function of the ideal UEG at (a) $\theta = 0.01$ and (b) $\theta = 0.02$ with the density parameter set to $r_s = 2$, and the wavenumber given in units of the Fermi wavenumber q_F . The solid line is the Lindhard function, while the dashed line corresponds to the analytic solution for the TF model. Symbols indicate data computed using OFDFT with an external harmonic perturbation and various non-interacting free energy functionals. Note that the results from the WTF and XWMF for $\chi_0^{(1)}(\mathbf{q})$ are almost identical.

If we use the approximation $\Gamma_{\text{RPA}}^{(3)}(\mathbf{q}) \simeq \Gamma_s^{(3)}(\mathbf{q})$ in Eq. (78), we derive the result from Ref. [15]:

$$\chi_{\text{RPA}}^{(3)}(\mathbf{q}) = \chi_0^{(3)}(\mathbf{q}) \left[1 - v(\mathbf{q})\chi_0^{(1)}(\mathbf{q}) \right]^{-3} \times \left[1 - v(3\mathbf{q})\chi_0^{(1)}(3\mathbf{q}) \right]^{-1}. \quad (79)$$

The approximations for $\chi^{(3)}(\mathbf{q})$ in the form of Eq. (77) and Eq. (79) were first presented in Ref. [15]. The presented derivations provide clarification regarding the approximations entering into Eq. (77) and Eq. (79). Eq. (77) and Eq. (79) are based on the approximations $\Gamma_{\text{tot}}^{(3)}(\mathbf{q}) \simeq \Gamma_s^{(3)}(\mathbf{q})$ and $\Gamma_{\text{RPA}}^{(3)}(\mathbf{q}) \simeq \Gamma_s^{(3)}(\mathbf{q})$, respectively.

III. APPLICATIONS

In this section, we demonstrate the application of the presented DFT framework by analyzing various non-interacting free energy functionals commonly used in orbital-free DFT (OFDFT). We specifically examine the Wang-Teter (WTF) functional [16, 17], the LKTF functional [18, 19], and the XWMF functional [20, 21]. To facilitate this analysis, we have implemented the LKTF, WTF, and XWMF non-interacting free energy functionals into the open-source code DFTpy [63].

Additionally, we conducted Kohn-Sham DFT (KS-DFT) calculations to generate exact data for the ideal non-linear density response functions. We consider the metallic electron density with a density parameter of $r_s = 2$, where r_s represents the mean inter-electron distance in units of the Bohr radius [64]. This density is typical for metals and warm dense matter applications. We

also vary the degeneracy parameter $\theta = k_B T / E_F$, where E_F is the Fermi energy, over the range from $\theta = 0.01$ to $\theta = 2$.

A. Details of the simulations

The OFDFT and KSDFT calculations of the ideal UEG perturbed by the external harmonic perturbation (25) were performed using DFTpy and Quantum ESPRESSO [65–68]. To introduce the external harmonic perturbation in Quantum ESPRESSO calculations, we used QEpy [69], which is a Python DFT engine for Quantum ESPRESSO-based nonstandard workflows.

In both OFDFT and KSDFT calculations, we utilized a real-space density grid with a spacing of 0.2 Bohr. The OFDFT calculations were conducted with 118 electrons in a cuboid with dimensions $L_y = L_z = 7.77$ Bohr and $L_x = 65.49$ Bohr. The same simulation cell containing 118 electrons was used for the KSDFT calculations at $\theta = 0.01$ with the number of bands set to $N_b = 80$, and using a $2 \times 60 \times 60$ k-point grid. For higher temperatures ($\theta = 0.25$, $\theta = 0.5$, $\theta = 1$, and $\theta = 2$), the KSDFT calculations were performed with $N = 38$ electrons in a cuboid with side lengths $L_y = L_z = 7.77$ Bohr and $L_x = 21.09$ Bohr. The k-point grid for these simulations was set to $4 \times 16 \times 16$. The number of bands was adjusted according to the temperature: $N_b = 140$ at $\theta = 0.25$, $N_b = 280$ at $\theta = 0.5$, $N_b = 600$ at $\theta = 1$, and $N_b = 1400$ at $\theta = 2$. In all KSDFT calculations, we applied a cutoff energy of 62 Ry.

B. Results of the calculations

B.1. Linear density response $\chi_0^{(1)}(\mathbf{q})$

To begin with, we consider the quality of $\chi_0^{(1)}(\mathbf{q})$ computed using different approximations for $F_s[n]$, as well as how $\chi_0^{(1)}(\mathbf{q})$ depends on wavenumber and temperature. Understanding these aspects, as we will see, is crucial for interpreting the results for the ideal non-linear density response functions.

In Fig. 1, for $\theta = 0.01$ and $\theta = 1.0$, we compare the OFDFT and KSDFT results for $\chi_0^{(1)}(\mathbf{q})$ with the Lindhard function (which is the exact solution for $\chi_0^{(1)}(\mathbf{q})$ of the ideal UEG). As expected, the KSDFT data show excellent agreement with the Lindhard function. The OFDFT calculations using the WTF and XWMF also reproduce the Lindhard function, as these functionals are designed to reduce to it in the UEG limit. The dependence of the GGA level LKTF result for the response function $\chi_0^{(1)}(\mathbf{q})$ on the wavenumber is also as anticipated [18, 19]. The LKTF result tends toward the TF limit at small wavenumbers and exhibits a decreasing magnitude as the wavenumber increases, with the quality aligning with the expectations from the $F_s[n]$ with a gradient correction [62, 70–73]. The TF result for $\chi_0^{(1)}(\mathbf{q})$ agrees

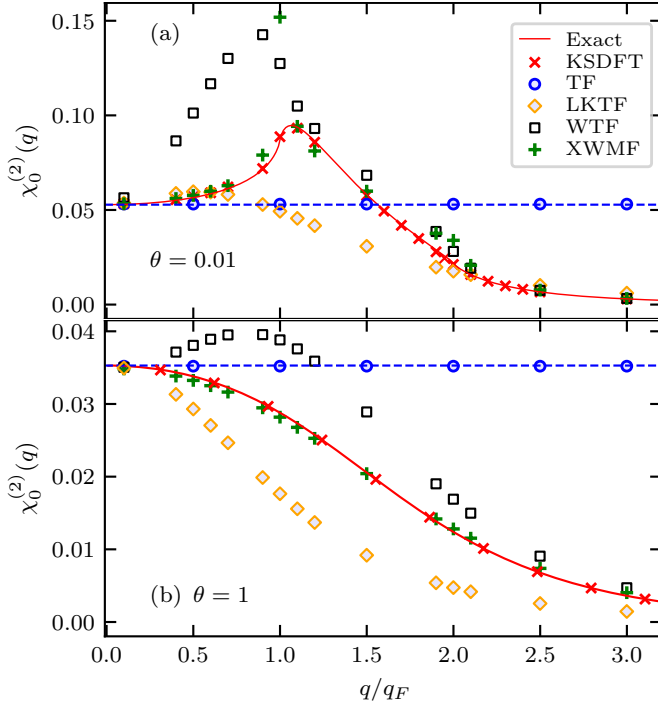


FIG. 2. Quadratic static density response function of the ideal UEG at (a) $\theta = 0.01$ and (b) $\theta = 1.0$ with the density parameter $r_s = 2$. The solid line represents the exact solution given by Eq. (43) and the dashed line shows the analytic solution using the TF model. Symbols correspond to the OFDFT calculations using the external harmonic perturbation and different approximations for the non-interacting free energy functional.

with the exact result in the limit $\mathbf{q} \rightarrow 0$ and remains constant regardless of the wavenumber of the perturbation. In addition, in Fig. 1, we see that the results from the TF model-based OFDFT simulations of the harmonically perturbed ideal electron gas (circles) are in agreement with the theoretical result using the second-order functional derivative of the TF functional (dashed horizontal lines). The latter is provided by Eq. (A1).

B.2. Quadratic density response $\chi_0^{(2)}(\mathbf{q})$

In Fig. 2, we present the results for the quadratic density response at the second harmonic, $\chi_0^{(2)}(\mathbf{q})$, at $\theta = 0.01$ and $\theta = 1.0$. We compare the results obtained from OFDFT and KSDFT with the exact solution (43) given by Mikhailov [33]. As it should be, the KSDFT data agree with the analytical solution (43). From Fig. 2(a), we observe that the exact solution for $\chi_0^{(2)}(\mathbf{q})$ exhibits a positive peak at approximately $q \simeq q_F$. The origin of this maximum can be understood by recalling that $\chi_0^{(2)}(\mathbf{q})$ is proportional to the difference $\chi_0^{(1)}(2\mathbf{q}) - \chi_0^{(1)}(\mathbf{q})$ (see Eq. 43). At $\theta = 0.01$, the slope of $\chi_0^{(1)}(\mathbf{q})$ has the largest value around $q = 2q_F$ (as one can see from Fig. 1(a)),

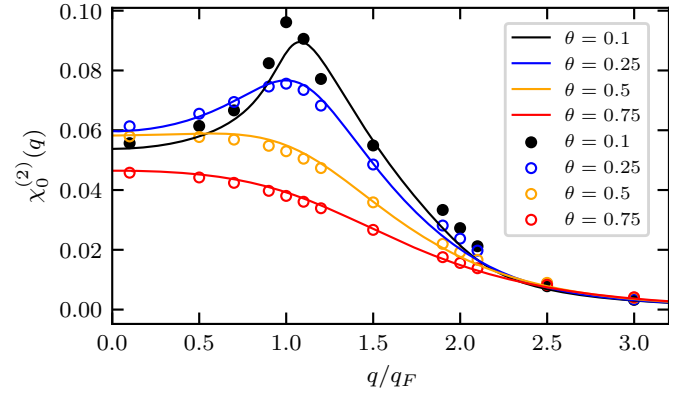


FIG. 3. Quadratic static density response function at second harmonic of the ideal UEG at different values of the degeneracy parameter with the density parameter set to $r_s = 2$. The lines correspond to the exact solution given by Eq. (43). Circles depict the results of the OFDFT calculations using the XWMF non-interacting free-energy functional.

while its q -dependence is much weaker for $q \ll q_F$ and $q \gtrsim 3q_F$. As a result, the difference $\chi_0^{(1)}(2\mathbf{q}) - \chi_0^{(1)}(\mathbf{q})$ increases most rapidly around $q \simeq q_F$, producing the pronounced peak observed in Fig. 2(a). As the temperature increases to $\theta = 1.0$, this peak disappears, as illustrated in Fig. 2(b). This results from the thermally induced reduction of the slope of $\chi_0^{(1)}(\mathbf{q})$ at $q = 2q_F$ (see Fig. 1(b)).

From Fig. 2, we see that for both $\theta = 0.01$ and $\theta = 1.0$, the results from the LKTF-based OFDFT calculations for $\chi_0^{(2)}(\mathbf{q})$ align well with the exact solution at the limits of small and large wavenumbers. However, at intermediate wavenumbers where $0.1 q_F \lesssim q \lesssim 2 q_F$, the LKTF data exhibits significant disagreement with the exact solution. While this behavior is expected for the LKTF, it is surprising to see that the WTF also performs poorly in describing $\chi_0^{(2)}(\mathbf{q})$. The WTF functional is specifically designed to reproduce $\chi_0^{(1)}(\mathbf{q})$, which is supported by simulations of the perturbed ideal UEG, as shown in Fig. 1. In principle, this should suffice for providing an accurate description of $\chi_0^{(2)}(\mathbf{q})$, as indicated by Eq. (43). However, Fig. 2 reveals that this is not the case for the WTF. This discrepancy clearly suggests that the ansatz used to construct the WTF functional violates the exact constraint given in Eq. (42). In contrast, XWMF, a functional developed using the method of line integrals and designed to reproduce the $\chi_0^{(1)}(\mathbf{q})$ of the ideal UEG, shows close agreement with the exact data for $\chi_0^{(2)}(\mathbf{q})$. The only exceptions are in the regions around $q = q_F$ and $q = 2q_F$ at $\theta = 0.01$. This behavior of XWMF is attributed to a numerical issue that arises when computing the ground state $\chi_0^{(1)}(\mathbf{q})$ at $q = 2q_F$. This issue stems from the term $f(z) = (1 - z^2) \ln \left| \frac{1+z}{1-z} \right|$ (where $z = \frac{q}{2q_F}$) in the Lindhard function [32, 74]. Although it is true that $\lim_{z \rightarrow 0} f(z) \rightarrow 0$ theoretically, numerically one has to use a finite value for the logarithm in $f(z)$ in the

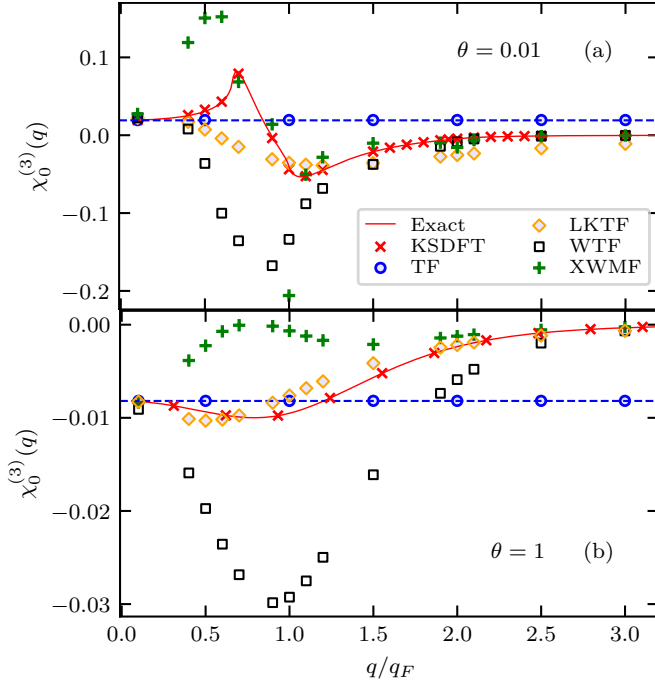


FIG. 4. Cubic static density response function of the ideal UEG at (a) $\theta = 0.01$ and (b) $\theta = 0.01$ with the density parameter $r_s = 2$. The solid line represents the exact solution given by Eq. (74) and the dashed line is the analytic solution using the TF model. Symbols correspond to the OFDFT calculations using the external harmonic perturbation and different approximations for the non-interacting free energy functional.

vicinity of $z = 1$. This numerical peculiarity has a negligible effect on $\chi_0^{(1)}(\mathbf{q})$, but it can lead to significant inaccuracies in $\chi_0^{(2)}(\mathbf{q})$ around $q = q_F$ and $q = 2q_F$, if not carefully treated. This is because $\chi_0^{(2)}(\mathbf{q})$ is proportional to the difference between $\chi_0^{(1)}(2\mathbf{q})$ and $\chi_0^{(1)}(\mathbf{q})$ (see Eq. (43)), which makes it more sensitive to the accuracy of the calculations. This issue diminishes at $\theta = 1$. At this condition with strong thermal excitations, $\chi_0^{(2)}(\mathbf{q})$ does not exhibit noticeable non-monotonic behavior (see Fig. 2(b)).

In Fig. 3, we present $\chi_0^{(2)}(\mathbf{q})$ at various values of θ to illustrate the correlation between the enhanced performance of the XWMF and the suppression of the maxima of $\chi_0^{(2)}(\mathbf{q})$ due to thermal excitations. From Fig. 3, it is evident that for $\theta \geq 0.25$, the XWMF results have a good agreement with the exact solution for $\chi_0^{(2)}(\mathbf{q})$ without significant issues around $q = q_F$ and $q = 2q_F$. Thus, in terms of describing the quadratic response function, the XWMF demonstrates superior performance under WDM conditions compared to other non-interacting free energy functionals that have been considered.

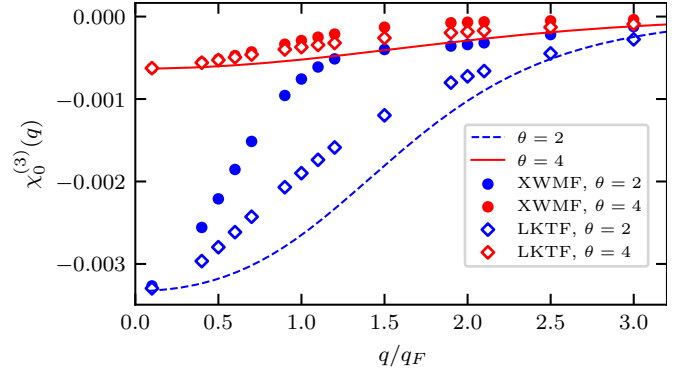


FIG. 5. Cubic static density response function at third harmonic of the ideal UEG at $\theta = 2$ and $\theta = 4$ with $r_s = 2$. The lines correspond to the exact solution given by Eq. (74). Symbols show the results of the OFDFT calculations using the XWMF and LKTF non-interacting free-energy functionals.

B.3. Cubic density response at third harmonic $\chi_0^{(3)}(\mathbf{q})$

In Fig. 4, the results for $\chi_0^{(3)}(\mathbf{q})$ at $\theta = 0.01$ and $\theta = 1$ are presented. As expected, the KSDFT calculations closely match the exact analytic solution in equation (74). At $\theta = 0.01$, $\chi_0^{(3)}(\mathbf{q})$ displays a pronounced positive peak around $q = \frac{2}{3}q_F$ and a negative minimum at $q = q_F$. The origin of this structure can be explained by looking at the recursive relation in equation (74). From this relation, we can see that $\chi_0^{(3)}(\mathbf{q})$ is determined by the combination $3\chi_0^{(1)}(3\mathbf{q}) - 8\chi_0^{(1)}(2\mathbf{q}) + 5\chi_0^{(1)}(\mathbf{q})$ of the ideal linear density response functions. This, combined with the sharp slope of $\chi_0^{(1)}(\mathbf{k})$ around $k = 2q_F$, results in a strong non-monotonic dependence of $\chi_0^{(3)}(\mathbf{q})$ on the wavenumber near $q = \frac{2}{3}q_F$ and $q = q_F$.

From Fig. 4, we can confirm that the TF result accurately provides the $q \rightarrow 0$ limit for $\chi_0^{(3)}(\mathbf{q})$. This is supported by the agreement between the analytic solution (depicted as horizontal dashed lines) and the simulation data for the perturbed electron gas (represented by circles). The analytic solution for the TF model is given by Eqs. (A2) and (A8). The data from the WTF-based OFDFT calculations for $\chi_0^{(3)}(\mathbf{q})$ align with the exact solution at both small and large wavenumbers. However, significant deviations are observed at intermediate wavenumbers, specifically in the range of $0.1q_F \lesssim q \lesssim 2q_F$. In comparison to the WTF, the LKTF model provides a much more accurate description of $\chi_0^{(3)}(\mathbf{q})$. Although LKTF is based on GGA, which, as expected, does not capture a sharp positive peak for $\chi_0^{(3)}(\mathbf{q})$ around $q \approx \frac{2}{3}q_F$, it does manage to identify a pattern with a negative minimum. Furthermore, Fig. 4 indicates that the XWMF performs worse for $\chi_0^{(3)}(\mathbf{q})$ compared to the cases of the ideal quadratic and linear density response functions. In fact, we can assess that LKTF is more accurate than XWMF for $\chi_0^{(3)}(\mathbf{q})$, par-

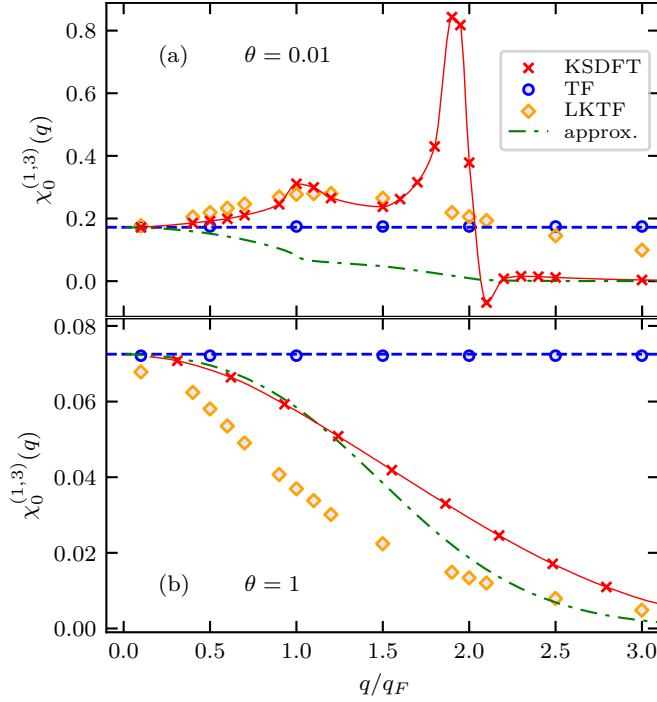


FIG. 6. Cubic static density response function of the ideal UEG at the first harmonic for (a) $\theta = 0.01$ and (b) $\theta = 1.0$, with density parameter $r_s = 2$. The KSDFT results are shown as cross markers, with an interpolated line included to guide the eye. The horizontal dashed line denotes the analytic Thomas–Fermi (TF) solution. Other symbols represent OFDFT calculations using different approximations to the non-interacting free-energy functional. The dash-dotted line depicts analytical approximation (68).

ticularly at $\theta = 1$ (as shown in Fig. 4(b)). This trend persists for larger values of θ , as illustrated in Fig. 5, which presents results for $\chi_0^{(3)}(\mathbf{q})$ computed at $\theta = 2$ and $\theta = 4$ using both LKTF and XWMF. The decline in the performance of the XWMF for $\chi_0^{(3)}(\mathbf{q})$, relative to the ideal quadratic and linear response functions, is likely due to the peculiarities of the line integrals used.

As a third-order contribution with respect to the magnitude of the perturbation, the poor performance of the XWMF and WTF for $\chi_0^{(3)}(\mathbf{q})$ does not allow for an adequate analysis of $\chi_0^{(1,3)}(\mathbf{q})$ when employing these functionals in simulations of the harmonically perturbed UEG.

B.4. Cubic density response at first harmonic $\chi_0^{(1,3)}(\mathbf{q})$

In Figure 6, we present the KSDFT results for $\chi_0^{(1,3)}(\mathbf{q})$ at two temperatures: $\theta = 0.01$ and $\theta = 1.0$. From Figure 6(a), it is clear that $\chi_0^{(1,3)}(\mathbf{q})$ exhibits a pronounced non-monotonic dependence on the perturbation wavenumber. Specifically, it features two peaks: one at approximately $q \simeq q_F$ and another at $q \simeq 1.85 q_F$, along

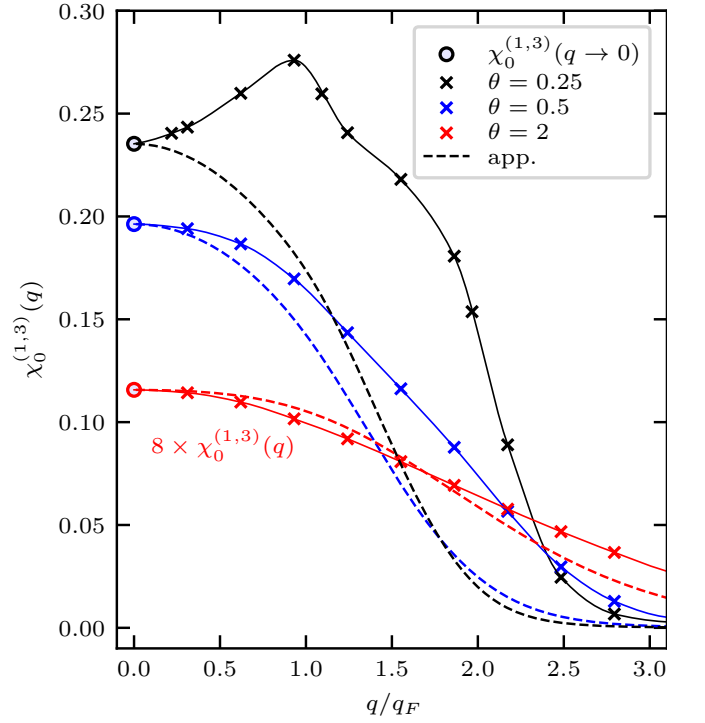


FIG. 7. Cubic static density response function at first harmonic of the ideal UEG at different values of the degeneracy parameters and $r_s = 2$. The KSDFT results are depicted using markers, with an interpolated line included to guide the eye. The dashed line corresponds to approximation (68).

with a negative minimum at $q \simeq 2.1 q_F$. Additionally, there is a notable drop from positive to negative values around $q = 2 q_F$. This non-monotonic behavior is similar to what is observed in the second- and third-order response functions, $\chi_0^{(2)}(\mathbf{q})$ and $\chi_0^{(3)}(\mathbf{q})$, at $\theta = 0.01$. For $\chi_0^{(1,3)}(\mathbf{q})$, the structure around $q = q_F$ and $q = 2 q_F$ can be traced back to the aforementioned peculiar feature of the linear response function $\chi_0^{(1)}(\mathbf{q})$ near twice the Fermi wavenumber, where the maximum slope (i.e., the maximum magnitude of its derivative) is located. As established in Eq. (61), $\chi_0^{(1,3)}(\mathbf{q})$ arises from mode coupling between density perturbations at $\mathbf{k} = \mathbf{q}$ and $\mathbf{k} = 2\mathbf{q}$. Consequently, strong non-monotonic features appear for perturbation wavenumbers at the Fermi wavenumber and its second harmonic.

The non-monotonic behavior of $\chi_0^{(1,3)}(\mathbf{q})$ disappears entirely as the temperature increases to $\theta = 1.0$, as shown in Figure 6(b). At this higher temperature, $\chi_0^{(1,3)}(\mathbf{q})$ becomes positive and decreases monotonically with increasing wavenumber.

From Fig. 6, we observe that for both temperatures, $\theta = 0.01$ and $\theta = 1.0$, the KSDFT data align with the TF results at small wavenumbers. Furthermore, we observe agreement between the exact analytical result (67) (also see (A6)) for the $\mathbf{q} \rightarrow 0$ limit of $\chi_0^{(1,3)}(\mathbf{q})$, derived using the TF model (indicated by the horizontal dashed line),

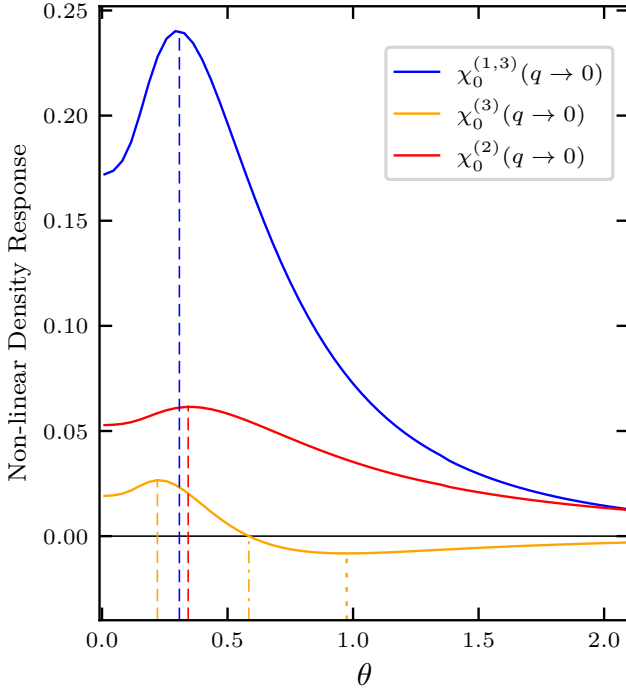


FIG. 8. The dependence of the long-wavelength limit of the ideal non-linear response functions of the UEG on the degeneracy parameter θ . The dashed vertical lines indicate the positions of the maxima of $\chi_0^{(1,3)}(q \rightarrow 0)$, $\chi_0^{(2)}(q \rightarrow 0)$, and $\chi_0^{(3)}(q \rightarrow 0)$. The dotted line represents the minimum of $\chi_0^{(3)}(q \rightarrow 0)$, while the dash-dotted line indicates the zero value of $\chi_0^{(3)}(q \rightarrow 0)$. The function $\chi_0^{(1,3)}(q \rightarrow 0)$ reaches its maximum value at $\theta \simeq 0.308$, and $\chi_0^{(2)}(q \rightarrow 0)$ reaches its maximum at $\theta \simeq 0.343$. Additionally, $\chi_0^{(3)}(q \rightarrow 0)$ has a maximum value at $\theta \simeq 0.22$, a minimum value at $\theta \simeq 0.975$, and crosses zero at $\theta \simeq 0.58$.

and the TF-based OFDFT simulations of the perturbed ideal UEG (shown as circles). At $\theta = 0.01$, the OFDFT results obtained using the LKTF functional provide a satisfactory description of $\chi_0^{(1,3)}(\mathbf{q})$ for $q \lesssim 1.5q_F$. However, the LKTF does not capture the strong non-monotonic features of $\chi_0^{(1,3)}(\mathbf{q})$ around $q = 2q_F$, which is beyond the capabilities of the GGA level description. At $\theta = 1.0$, the LKTF also demonstrates a monotonically decreasing trend with increasing wavenumber. While it is quantitatively accurate at both small and large wavenumbers, the LKTF shows disagreement with the KSDF data in the intermediate range.

In Fig. 6, we also compare approximation (68) with the KSDF data. It can be seen that Eq. (68) (dash-dotted line) does not capture the non-monotonic behavior of $\chi_0^{(1,3)}(\mathbf{q})$ at $\theta = 0.01$, and it provides quantitative agreement with the KSDF results only in the limit of small wavenumbers, where $\chi_0^{(1,3)}(\mathbf{q})$ values are close to the TF data. At $\theta = 1.0$, the approximation (68) adequately captures the monotonically decreasing pattern of $\chi_0^{(1,3)}(\mathbf{q})$ and yields quantitatively accurate results for

$q \lesssim q_F$.

In Fig. 7, we present KSDF data for $\chi_0^{(1,3)}(\mathbf{q})$ at $\theta = 0.25$, $\theta = 0.5$, and $\theta = 2$. The values of $\chi_0^{(1,3)}(\mathbf{q})$ at the limit $\mathbf{q} \rightarrow 0$ are computed using the derived exact analytical result (67). We clearly see the thermal excitations induced suppression of the non-monotonic behavior of $\chi_0^{(1,3)}(\mathbf{q})$. At $\theta = 0.25$, $\chi_0^{(1,3)}(\mathbf{q})$ exhibits only one maximum and does not reach any negative values. Further increasing θ to $\theta = 0.5$ leads to a monotonically decreasing behavior of $\chi_0^{(1,3)}(\mathbf{q})$ as the wavenumber increases. Moreover, the rate of decrease of $\chi_0^{(1,3)}(\mathbf{q})$ with increasing wavenumber slows down as θ increases, as illustrated by the result for $\theta = 2$ in Fig. 7 and $\theta = 1$ in Fig. 6. As θ increases, the quality of approximation (68) improves, leading to a better quantitative description of $\chi_0^{(1,3)}(\mathbf{q})$.

In Fig. 8, we illustrate how the $\mathbf{q} \rightarrow 0$ limits of the examined non-linear density response functions depend on the degeneracy parameter θ . As discussed in Appendix A, the small- \mathbf{q} limits of $\chi_0^{(2)}(\mathbf{q})$, $\chi_0^{(3)}(\mathbf{q})$, and $\chi_0^{(1,3)}(\mathbf{q})$ depend solely on θ . From Fig. 8, it is evident that these limits exhibit a non-monotonic dependence on θ : all three functions initially increase with increasing θ , reach a positive maximum, and then decrease as θ continues to rise. Quantitatively, $\chi_0^{(1,3)}(q \rightarrow 0)$ attains its maximum at $\theta \simeq 0.308$, while $\chi_0^{(2)}(q \rightarrow 0)$ reaches its maximum at $\theta \simeq 0.343$. The cubic response at the third harmonic, $\chi_0^{(3)}(q \rightarrow 0)$, shows a maximum at $\theta \simeq 0.22$, a minimum at $\theta \simeq 0.975$, and crosses zero near $\theta \simeq 0.58$. These trends indicate that non-linear electronic response effects are most pronounced for partially degenerate electrons with $\theta < 0.5$.

IV. CONCLUSIONS AND OUTLOOK

We investigated the relationship between static non-linear density response functions and the functional derivatives of free-energy functionals. For systems with an average homogeneous density distribution, Eq. (23) provides a general DFT-based framework for describing the non-linear response of electrons. This framework allowed us to uncover the underlying mode-coupling structure responsible for the previously unresolved cubic response at the first harmonic. For the ideal UEG, it also yields exact analytical long-wavelength limits for all non-linear response functions considered. The resulting connection between $F_s[n]$ and the ideal non-linear response functions provides useful constraints for constructing non-interacting free-energy functionals.

As a practical application, we emphasize that a key element in developing approximations to the non-interacting free-energy functionals for metals, semiconductors, and warm dense matter is the link between the ideal linear density response function of the UEG and the second-order functional derivative of $F_s[n]$, given by Eq. (34). At low temperatures ($T \rightarrow 0$), $F_s[n]$ reduces to

the kinetic-energy functional. In a similar way, Eqs. (42) and (75), which connect the third- and fourth-order functional derivatives of $F_s[n]$ to $\chi_0^{(2)}(\mathbf{q})$ and $\chi_0^{(3)}(\mathbf{q})$, provide additional exact constraints. These constraints can be useful when selecting or validating an ansatz for constructing a particular approximation for $F_s[n]$. This is motivated by the fact that the quadratic density response at the second harmonic, $\chi_0^{(2)}(\mathbf{q})$, and the cubic response at the third harmonic, $\chi_0^{(3)}(\mathbf{q})$, can be expressed as combinations of ideal linear density response functions [34, 35] (see Eqs. (43) and (74)).

Our OFDFT simulations show that the WTF functional, although it reproduces $\chi_0^{(1)}(\mathbf{q})$, violates the exact quadratic-response relation and therefore fails to describe $\chi_0^{(2)}(\mathbf{q})$ across the relevant wave-number range. In contrast, the XWMF functional provides a reasonable description of the quadratic response. Both the WTF and XWMF functionals, however, fail to capture the cubic density response at the first and third harmonics. The LKTF functional performs more robustly, although it cannot reproduce the sharp non-monotonic features in the ideal non-linear response that arise from the steep slope of the Lindhard function near $2q_F$ in the strongly degenerate regime ($\theta \ll 1$). Approximations to $F_s[n]$ that accurately describe non-linear density responses are expected to be important in the warm dense matter regime, at parameters where an accurate treatment of electron screening of ion-ion pair interaction potential requires going beyond the linear-response regime [46, 75–77]. In this context, satisfying the quadratic-response constraint of Eq. (43) is particularly important, as it represents the next leading contribution after the linear response [15].

Using our framework, we have also obtained the first exact KSDFD data for $\chi_0^{(1,3)}(\mathbf{q})$ in the UEG. These results reveal strong non-monotonic features at low temperature that originate from mode coupling between perturbations at \mathbf{q} and $2\mathbf{q}$. These structures gradually diminish with increasing temperature and become fully monotonic for $\theta \gtrsim 0.5$. We also find that the exact long-wavelength limits of all non-linear response functions exhibit a non-monotonic dependence on the degeneracy parameter, indicating that non-linear effects are strongest for partially degenerate electrons with $\theta < 0.5$.

Overall, the present work establishes a systematic route for using non-linear response theory to inform the development, evaluation, and refinement of orbital-free DFT functionals. Future applications include constructing constrained non-interacting functionals consistent with the hierarchy of ideal response relations. Another promising direction is extending constraints for exchange–correlation functionals by incorporating exact results for the kernel $\tilde{\chi}_{xc}^{(3)}(2\mathbf{q}|\mathbf{q},\mathbf{q})$ (see Eq. (47)), which can be computed using various quantum Monte Carlo methods [23, 25]. Finally, the framework can also be used to investigate time-dependent non-linear response in warm dense matter and quantum plasmas by analyz-

ing the electronic response to perturbations of the form $\Delta v_{\text{ext}} \propto \cos(\mathbf{q} \cdot \mathbf{r} - \omega t)$.

ACKNOWLEDGMENTS

This work was partially supported by the Center for Advanced Systems Understanding (CASUS), financed by Germany’s Federal Ministry of Education and Research (BMBF) and the Saxon state government out of the State budget approved by the Saxon State Parliament. This work has received funding from the European Research Council (ERC) under the European Union’s Horizon 2022 research and innovation programme (Grant agreement No. 101076233, ”PREXTREME”). Views and opinions expressed are however those of the authors only and do not necessarily reflect those of the European Union or the European Research Council Executive Agency. Neither the European Union nor the granting authority can be held responsible for them. Tobias Dornheim gratefully acknowledges funding from the Deutsche Forschungsgemeinschaft (DFG) via project DO 2670/1-1. Computations were performed on a Bull Cluster at the Center for Information Services and High-Performance Computing (ZIH) at Technische Universität Dresden and at the Norddeutscher Verbund für Hoch- und Höchstleistungsrechnen (HLRN) under grant mvp00024.

Appendix A: Thomas–Fermi reduced kernels

For the TF potential $v_{\text{TF}}[n] = \mu(\eta[n])$ [78], the reduced kernels read:

$$\tilde{\chi}_{\text{TF}}^{(2)} = \frac{1}{\beta} \frac{\lambda_T^3}{g} \frac{1}{F_{-1/2}(\eta)}, \quad (\text{A1})$$

$$\tilde{\chi}_{\text{TF}}^{(3)} = -\frac{1}{2} \frac{1}{\beta} \left(\frac{\lambda_T^3}{g} \right)^2 \frac{F_{-3/2}(\eta)}{[F_{-1/2}(\eta)]^3}, \quad (\text{A2})$$

$$\tilde{\chi}_{\text{TF}}^{(4)} = \frac{1}{6} \frac{1}{\beta} \left(\frac{\lambda_T^3}{g} \right)^3 \frac{3 [F_{-3/2}(\eta)]^2 - F_{-1/2}(\eta) F_{-5/2}(\eta)}{[F_{-1/2}(\eta)]^5}, \quad (\text{A3})$$

where $\lambda_T = \sqrt{2\pi\beta}$, $\beta = 1/T$, $g = 2$, $\eta = \mu\beta$, and $F_\nu(\eta)$ is the Fermi integral of order ν . We calculated the Fermi integrals using $F_\nu(\eta) = -\text{Li}_{\nu+1}(-e^\eta)$, with the polylogarithm computed using the Python mpmath library.

The chemical potential $\eta = \mu\beta$ is defined by the temperature and density through the relation:

$$\frac{2}{3} \theta^{-3/2} = \int_0^\infty \frac{\sqrt{x}}{1 + \exp(x - \eta)} dx, \quad (\text{A4})$$

with $\theta = T/E_F = 2T/(3\pi^2 n)^{2/3}$ being the degeneracy parameter.

Eq. (A1) defines the long wavelength limit of the ideal density response function $\chi_0^{(1)}(\mathbf{q} \rightarrow 0) = -1/\tilde{\kappa}_{\text{TF}}^{(2)}$. Using Eq. (39) and the TF reduced kernels, for the long wavelength limit of the ideal quadratic density response function, we find:

$$\chi^{(2)}(\mathbf{q} \rightarrow 0) = -\frac{\tilde{\kappa}_{\text{TF}}^{(3)}}{[\tilde{\kappa}_{\text{TF}}^{(2)}]^3}. \quad (\text{A5})$$

Following Eq. (67), for the cubic response at first harmonic, we have:

$$\chi_0^{(1,3)}(\mathbf{q} \rightarrow 0) = \frac{\Gamma_{\text{TF}}^{(1,3)}}{[\tilde{\kappa}_{\text{TF}}^{(2)}]^4}, \quad (\text{A6})$$

where

$$\Gamma_{\text{TF}}^{(1,3)}(\mathbf{q}) = \tilde{\kappa}_{\text{TF}}^{(4)} - 2 \frac{[\tilde{\kappa}_{\text{TF}}^{(3)}]^2}{\tilde{\kappa}_{\text{TF}}^{(2)}}. \quad (\text{A7})$$

Using Eq. (73) and the TF kernels, for the cubic response at third harmonic, we have:

$$\chi_0^{(3)}(\mathbf{q} \rightarrow 0) = \frac{\Gamma_{\text{TF}}^{(3)}}{[\tilde{\kappa}_{\text{TF}}^{(2)}]^4}, \quad (\text{A8})$$

where

$$\Gamma_{\text{TF}}^{(3)}(\mathbf{q}) = -\frac{[\tilde{\kappa}_{\text{TF}}^{(3)}]^2}{\tilde{\kappa}_{\text{TF}}^{(2)}} + \tilde{\kappa}_{\text{TF}}^{(4)}. \quad (\text{A9})$$

-
- [1] R. O. Jones, “Density functional theory: Its origins, rise to prominence, and future,” *Rev. Mod. Phys.* **87**, 897–923 (2015).
 - [2] J.P. Hansen and I.R. McDonald, *Theory of simple liquids : with applications to soft matter* (Academic Press, 2013).
 - [3] Jan Vorberger, Tobias Dornheim, Maximilian P. Böhme, Zhandos A. Moldabekov, and Panagiotis Tolias, “Green’s function perspective on the nonlinear density response of quantum many-body systems,” *Journal of Statistical Physics* **192**, 75 (2025).
 - [4] Tobias Dornheim, Jan Vorberger, and Zhandos A. Moldabekov, “Nonlinear density response and higher order correlation functions in warm dense matter,” *Journal of the Physical Society of Japan* **90**, 104002 (2021).
 - [5] Tobias Dornheim, Zhandos A. Moldabekov, Kushal Ramakrishna, Panagiotis Tolias, Andrew D. Baczewski, Dominik Kraus, Thomas R. Preston, David A. Chapman, Maximilian P. Böhme, Tilo Döppner, Frank Graziani, Michael Bonitz, Attila Cangi, and Jan Vorberger, “Electronic density response of warm dense matter,” *Physics of Plasmas* **30** (2023), 10.1063/5.0138955, 032705.
 - [6] M.A.L. Marques, N.T. Maitra, F.M.S. Nogueira, E.K.U. Gross, and A. Rubio, *Fundamentals of Time-Dependent Density Functional Theory*, Lecture Notes in Physics (Springer Berlin Heidelberg, 2012).
 - [7] E. K. U. Gross and Walter Kohn, “Local density-functional theory of frequency-dependent linear response,” *Phys. Rev. Lett.* **55**, 2850–2852 (1985).
 - [8] Zhandos Moldabekov, Jan Vorberger, and Tobias Dornheim, “Density functional theory perspective on the nonlinear response of correlated electrons across temperature regimes,” *Journal of Chemical Theory and Computation* **18**, 2900–2912 (2022), pMID: 35484932, <https://doi.org/10.1021/acs.jctc.2c00012>.
 - [9] A. Pribram-Jones, P. E. Grabowski, and K. Burke, “Thermal density functional theory: Time-dependent linear response and approximate functionals from the fluctuation-dissipation theorem,” *Phys. Rev. Lett* **116**, 233001 (2016).
 - [10] Christopher E. Patrick and Kristian S. Thygesen, “Adiabatic-connection fluctuation-dissipation dft for the structural properties of solids—the renormalized alda and electron gas kernels,” *The Journal of Chemical Physics* **143**, 102802 (2015), <https://doi.org/10.1063/1.4919236>.
 - [11] Wenhui Mi, Kai Luo, S. B. Trickey, and Michele Pavanello, “Orbital-free density functional theory: An attractive electronic structure method for large-scale first-principles simulations,” *Chemical Reviews* **123**, 12039–12104 (2023), pMID: 37870767, <https://doi.org/10.1021/acs.chemrev.2c00758>.
 - [12] Panagiotis Tolias, Tobias Dornheim, Zhandos A. Moldabekov, and Jan Vorberger, “Unravelling the nonlinear ideal density response of many-body systems,” *Europhysics Letters* **142**, 44001 (2023).
 - [13] William C. Witt and Emily A. Carter, “Kinetic energy density of nearly free electrons. i. response functionals of the external potential,” *Phys. Rev. B* **100**, 125106 (2019).
 - [14] S. Moroni, D. M. Ceperley, and G. Senatore, “Static response from quantum Monte Carlo calculations,” *Phys. Rev. Lett* **69**, 1837 (1992).
 - [15] Tobias Dornheim, Maximilian Böhme, Zhandos A. Moldabekov, Jan Vorberger, and Michael Bonitz, “Density response of the warm dense electron gas beyond linear response theory: Excitation of harmonics,” *Phys. Rev. Research* **3**, 033231 (2021).
 - [16] Lin-Wang Wang and Michael P. Teter, “Kinetic-energy functional of the electron density,” *Phys. Rev. B* **45**, 13196–13220 (1992).

- [17] Travis Sjostrom and Jérôme Daligault, “Nonlocal orbital-free noninteracting free-energy functional for warm dense matter,” *Phys. Rev. B* **88**, 195103 (2013).
- [18] K. Luo, V. V. Karasiev, and S. B. Trickey, “Towards accurate orbital-free simulations: A generalized gradient approximation for the noninteracting free energy density functional,” *Phys. Rev. B* **101**, 075116 (2020).
- [19] Kai Luo, Valentin V. Karasiev, and S. B. Trickey, “A simple generalized gradient approximation for the noninteracting kinetic energy density functional,” *Phys. Rev. B* **98**, 041111 (2018).
- [20] Cheng Ma, Min Chen, Yu Xie, Qiang Xu, Wenhui Mi, Yanchao Wang, and Yanming Ma, “Nonlocal free-energy density functional for a broad range of warm dense matter simulations,” *Phys. Rev. B* **110**, 085113 (2024).
- [21] Qiang Xu, Yanchao Wang, and Yanming Ma, “Nonlocal kinetic energy density functional via line integrals and its application to orbital-free density functional theory,” *Phys. Rev. B* **100**, 205132 (2019).
- [22] Dominik Kraus, Thomas R. Preston, and Ulf Zastrau, “Warm dense matter studies with x-ray free-electron lasers,” *Nature Reviews Physics* (2025), 10.1038/s42254-025-00893-7.
- [23] T. Dornheim, S. Groth, and M. Bonitz, “The uniform electron gas at warm dense matter conditions,” *Phys. Reports* **744**, 1–86 (2018).
- [24] F. Graziani, M. P. Desjarlais, R. Redmer, and S. B. Trickey, eds., *Frontiers and Challenges in Warm Dense Matter* (Springer, International Publishing, 2014).
- [25] Michael Bonitz, Jan Vorberger, Mandy Bethkenhagen, Maximilian P. Böhme, David M. Ceperley, Alexey Filinov, Thomas Gawne, Frank Graziani, Gianluca Gregori, Paul Hamann, Stephanie B. Hansen, Markus Holzmann, S. X. Hu, Hanno Kählert, Valentin V. Karasiev, Uwe Kleinschmidt, Linda Kordts, Christopher Makait, Burkhard Militzer, Zhandos A. Moldabekov, Carlo Pierleoni, Martin Preising, Kushal Ramakrishna, Ronald Redmer, Sebastian Schwalbe, Pontus Svensson, and Tobias Dornheim, “Toward first principles-based simulations of dense hydrogen,” *Physics of Plasmas* **31**, 110501 (2024), <https://pubs.aip.org/aip/pop/article-pdf/doi/10.1063/5.0219405/20250831/110501.1.5.0219405.pdf>.
- [26] Zhandos Moldabekov, Jan Vorberger, and Tobias Dornheim, “From density response to energy functionals and back: An ab initio perspective on matter under extreme conditions,” *Progress in Particle and Nuclear Physics* **140**, 104144 (2025).
- [27] M. Bonitz, T. Dornheim, Zh. A. Moldabekov, S. Zhang, P. Hamann, H. Kählert, A. Filinov, K. Ramakrishna, and J. Vorberger, “Ab initio simulation of warm dense matter,” *Physics of Plasmas* **27**, 042710 (2020).
- [28] Jan Vorberger, Frank Graziani, David Riley, Andrew D. Baczewski, Isabelle Baraffe, Mandy Bethkenhagen, Simon Blouin, Maximilian P. Böhme, Michael Bonitz, Michael Bussmann, Alexis Casner, Witold Cayzac, Peter Celliers, Gilles Chabrier, Nicolas Chamel, Dave Chapman, Mohan Chen, Jean Clérouin, Gilbert Collins, Federica Coppari, Tilo Döppner, Tobias Dornheim, Luke B. Fletcher, Dirk O. Gericke, Siegfried Glenzer, Alexander F. Goncharov, Gianluca Gregori, Sebastien Hamel, Stephanie B. Hansen, Nicholas J. Hartley, Suxing Hu, Omar A. Hurricane, Valentin V. Karasiev, Joshua J. Kas, Brendan Kettle, Thomas Kluge, Marcus D. Knudson, Alina Kononov, Zuzana Konôpková, Dominik Kraus, Andrea Kritcher, Sophia Malko, Gérard Mascarié, Burkhard Militzer, Zhandos A. Moldabekov, Michael S. Murillo, Bob Nagler, Nadine Nettelmann, Paul Neumayer, Benjamin K. Ofori-Okai, Ivan I. Oleynik, Martin Preising, Aurora Pribram-Jones, Tlekkabul Ramazanov, Alessandra Ravasio, Ronald Redmer, Baerbel Rethfeld, Alex P. L. Robinson, Gerd Röpke, François Soubiran, Charles E. Starrett, Gerd Steinle-Neumann, Phillip A. Sterne, Shigenori Tanaka, Aidan P. Thompson, Samuel B. Trickey, Tommaso Vinci, Sam M. Vinko, Lei Wang, Alexander J. White, Thomas G. White, Ulf Zastrau, Eva Zurek, and Panagiotis Tolias, “Roadmap for warm dense matter physics,” (2025), [arXiv:2505.02494 \[physics.plasm-ph\]](https://arxiv.org/abs/2505.02494).
- [29] Qiang Xu, Cheng Ma, Wenhui Mi, Yanchao Wang, and Yanming Ma, “Recent advancements and challenges in orbital-free density functional theory,” *WIREs Computational Molecular Science* **14**, e1724 (2024), <https://wires.onlinelibrary.wiley.com/doi/pdf/10.1002/wcms.1724>.
- [30] Zhandos A. Moldabekov, Xuecheng Shao, Michele Pavanello, Jan Vorberger, Frank Graziani, and Tobias Dornheim, “Imposing correct jellium response is key to predict the density response by orbital-free dft,” *Phys. Rev. B* **108**, 235168 (2023).
- [31] Zhandos A. Moldabekov, Xuecheng Shao, Michele Pavanello, Jan Vorberger, and Tobias Dornheim, “Nonlocal vs local pseudopotentials affect kinetic energy kernels in orbital-free dft,” *Electronic Structure* **7**, 015006 (2025).
- [32] J. Lindhard, “On the properties of a gas of charged particles,” *Matematisk-fysiske Meddelelser* **28**, 1–57 (1954).
- [33] S.A. Mikhailov, “Second-order response of a uniform three-dimensional electron gas to a longitudinal electric field,” *Annalen der Physik* **524**, 182–187 (2012).
- [34] S.A. Mikhailov, “Second-order response of a uniform three-dimensional electron gas to a longitudinal electric field,” *Annalen der Physik* **524**, 182–187 (2012), <https://onlinelibrary.wiley.com/doi/pdf/10.1002/andp.201100260>.
- [35] S. A. Mikhailov, “Nonlinear electromagnetic response of a uniform electron gas,” *Phys. Rev. Lett.* **113**, 027405 (2014).
- [36] Tobias Dornheim, Jan Vorberger, and Michael Bonitz, “Nonlinear electronic density response in warm dense matter,” *Phys. Rev. Lett.* **125**, 085001 (2020).
- [37] Tobias Dornheim, Zhandos A. Moldabekov, and Jan Vorberger, “Nonlinear electronic density response of the ferromagnetic uniform electron gas at warm dense matter conditions,” *Contributions to Plasma Physics*, e202100098 (2021).
- [38] Tobias Dornheim, Jan Vorberger, Zhandos A. Moldabekov, and Michael Bonitz, “Nonlinear interaction of external perturbations in warm dense matter,” *Contributions to Plasma Physics* **n/a**, e202100247.
- [39] Tobias Dornheim, Zhandos A. Moldabekov, and Jan Vorberger, “Nonlinear density response from imaginary-time correlation functions: Ab initio path integral monte carlo simulations of the warm dense electron gas,” *The Journal of Chemical Physics* **155**, 054110 (2021).
- [40] Zhandos A. Moldabekov, Jan Vorberger, Mani Lokamani, and Tobias Dornheim, “Averaging over atom snapshots in linear-response TDDFT of disordered systems: A case study of warm dense hydrogen,” *The Journal of Chemical Physics* **159**, 014107 (2023).
- [41] Carsten A. Ullrich, *Time-Dependent Density-Functional Theory: Concepts and Applications* (Oxford University

- Press, 2011).
- [42] Zhandos A. Moldabekov, Michele Pavanello, Maximilian P. Böhme, Jan Vorberger, and Tobias Dornheim, “Linear-response time-dependent density functional theory approach to warm dense matter with adiabatic exchange-correlation kernels,” *Phys. Rev. Res.* **5**, 023089 (2023).
 - [43] Zhandos Moldabekov, Maximilian Böhme, Jan Vorberger, David Blaschke, and Tobias Dornheim, “Ab Initio Static Exchange–Correlation Kernel across Jacob’s Ladder without Functional Derivatives,” *Journal of Chemical Theory and Computation* **19**, 1286–1299 (2023).
 - [44] Christian Kollmar and Frank Neese, “The static response function in kohn-sham theory: An appropriate basis for its matrix representation in case of finite ao basis sets,” *The Journal of Chemical Physics* **141**, 134106 (2014).
 - [45] G. Giuliani and G. Vignale, *Quantum Theory of the Electron Liquid* (Cambridge University Press, Cambridge, 2008).
 - [46] Kazutaka Nagao, S. A. Bonev, A. Bergara, and N. W. Ashcroft, “Enhanced friedel structure and proton pairing in dense solid hydrogen,” *Phys. Rev. Lett.* **90**, 035501 (2003).
 - [47] A. A. Kugler, “Theory of the local field correction in an electron gas,” *J. Stat. Phys.* **12**, 35 (1975).
 - [48] T. Dornheim, J. Vorberger, S. Groth, N. Hoffmann, Zh.A. Moldabekov, and M. Bonitz, “The static local field correction of the warm dense electron gas: An ab initio path integral Monte Carlo study and machine learning representation,” *J. Chem. Phys.* **151**, 194104 (2019).
 - [49] Tobias Dornheim, Sebastian Schwalbe, Panagiotis Tolias, Maximilian P. Böhme, Zhandos A. Moldabekov, and Jan Vorberger, “Ab initio density response and local field factor of warm dense hydrogen,” *Matter and Radiation at Extremes* **9**, 057401 (2024), https://pubs.aip.org/aip/mre/article-pdf/doi/10.1063/5.0211407/20079329/057401_1.5.0211407.pdf.
 - [50] J. M. Pitarke, R. H. Ritchie, and P. M. Echenique, “Quadratic response theory of the energy loss of charged particles in an electron gas,” *Phys. Rev. B* **52**, 13883–13902 (1995).
 - [51] C. D. Hu and E. Zaremba, “ Z^3 correction to the stopping power of ions in an electron gas,” *Phys. Rev. B* **37**, 9268–9277 (1988).
 - [52] Zhandos A. Moldabekov, Mani Lokamani, Jan Vorberger, Attila Cangi, and Tobias Dornheim, “Non-empirical Mixing Coefficient for Hybrid XC Functionals from Analysis of the XC Kernel,” *The Journal of Physical Chemistry Letters* **14**, 1326–1333 (2023).
 - [53] Zhandos Moldabekov, Tobias Dornheim, Jan Vorberger, and Attila Cangi, “Benchmarking exchange-correlation functionals in the spin-polarized inhomogeneous electron gas under warm dense conditions,” *Phys. Rev. B* **105**, 035134 (2022).
 - [54] Zhandos A. Moldabekov, Mani Lokamani, Jan Vorberger, Attila Cangi, and Tobias Dornheim, “Assessing the accuracy of hybrid exchange-correlation functionals for the density response of warm dense electrons,” *The Journal of Chemical Physics* **158**, 094105 (2023).
 - [55] Zhandos Moldabekov, Tobias Dornheim, Maximilian Böhme, Jan Vorberger, and Attila Cangi, “The relevance of electronic perturbations in the warm dense electron gas,” *The Journal of Chemical Physics* **155**, 124116 (2021), <https://doi.org/10.1063/5.0062325>.
 - [56] Maximilian Böhme, Zhandos A. Moldabekov, Jan Vorberger, and Tobias Dornheim, “Static electronic density response of warm dense hydrogen: Ab initio path integral monte carlo simulations,” *Phys. Rev. Lett.* **129**, 066402 (2022).
 - [57] S. Groth, T. Dornheim, T. Sjostrom, F. D. Malone, W. M. C. Foulkes, and M. Bonitz, “Ab initio exchange–correlation free energy of the uniform electron gas at warm dense matter conditions,” *Phys. Rev. Lett.* **119**, 135001 (2017).
 - [58] Valentin V. Karasiev, Travis Sjostrom, James Dufty, and S. B. Trickey, “Accurate homogeneous electron gas exchange-correlation free energy for local spin-density calculations,” *Phys. Rev. Lett.* **112**, 076403 (2014).
 - [59] John P. Perdew and Yue Wang, “Accurate and simple analytic representation of the electron-gas correlation energy,” *Phys. Rev. B* **45**, 13244–13249 (1992).
 - [60] J. P. Perdew and Alex Zunger, “Self-interaction correction to density-functional approximations for many-electron systems,” *Phys. Rev. B* **23**, 5048–5079 (1981).
 - [61] F. Perrot, “Gradient correction to the statistical electronic free energy at nonzero temperatures: Application to equation-of-state calculations,” *Phys. Rev. A* **20**, 586–594 (1979).
 - [62] D A Kirzhnits, Yurii E Lozovik, and Galina V Shpatakovskaya, “Statistical model of matter,” *Soviet Physics Uspekhi* **18**, 649 (1975).
 - [63] Xuecheng Shao, Kaili Jiang, Wenhui Mi, Alessandro Genova, and Michele Pavanello, “Dftpy: An efficient and object-oriented platform for orbital-free dft simulations,” *WIREs Computational Molecular Science* **11**, e1482 (2021), <https://wires.onlinelibrary.wiley.com/doi/pdf/10.1002/wcms.1482>.
 - [64] Torben Ott, Hauke Thomsen, Jan Willem Abraham, Tobias Dornheim, and Michael Bonitz, “Recent progress in the theory and simulation of strongly correlated plasmas: phase transitions, transport, quantum, and magnetic field effects,” *The European Physical Journal D* **72**, 84 (2018).
 - [65] Paolo Giannozzi, Stefano Baroni, Nicola Bonini, Matteo Calandra, Roberto Car, Carlo Cavazzoni, Davide Ceresoli, Guido L Chiarotti, Matteo Cococcioni, Ismaila Dabo, Andrea Dal Corso, Stefano de Gironcoli, Stefano Fabris, Guido Fratesi, Ralph Gebauer, Uwe Gerstmann, Christos Gougoussis, Anton Kokalj, Michele Lazzeri, Layla Martin-Samos, Nicola Marzari, Francesco Mauri, Riccardo Mazzarello, Stefano Paolini, Alfredo Pasquarello, Lorenzo Paulatto, Carlo Sbraccia, Sandro Scandolo, Gabriele Sclauzero, Ari P Seitsonen, Alexander Smogunov, Paolo Umari, and Renata M Wentzcovitch, “Quantum espresso: a modular and open-source software project for quantum simulations of materials,” *Journal of Physics: Condensed Matter* **21**, 395502 (2009).
 - [66] P Giannozzi, O Andreussi, T Brumme, O Bunau, M Buongiorno Nardelli, M Calandra, R Car, C Cavazzoni, D Ceresoli, M Cococcioni, N Colonna, I Carnimeo, A Dal Corso, S de Gironcoli, P Delugas, R A DiStasio, A Ferretti, A Floris, G Fratesi, G Fugallo, R Gebauer, U Gerstmann, F Giustino, T Gorni, J Jia, M Kawamura, H-Y Ko, A Kokalj, E Küçükbenli, M Lazzeri, M Marsili, N Marzari, F Mauri, N L Nguyen, H-V Nguyen, A Otero-de-la Roza, L Paulatto, S Poncé, D Rocca, R Sabatini, B Santra, M Schlipf, A P Seitsonen, A Smogunov, I Tim-

- rov, T Thonhauser, P Umari, N Vast, X Wu, and S Baroni, “Advanced capabilities for materials modelling with quantum espresso,” *Journal of Physics: Condensed Matter* **29**, 465901 (2017).
- [67] Paolo Giannozzi, Oscar Basergio, Pietro Bonfà, Davide Brunato, Roberto Car, Ivan Carnimeo, Carlo Cavazzoni, Stefano de Gironcoli, Pietro Delugas, Fabrizio Ferrari Ruffino, Andrea Ferretti, Nicola Marzari, Iurii Timrov, Andrea Urru, and Stefano Baroni, “Quantum espresso toward the exascale,” *The Journal of Chemical Physics* **152**, 154105 (2020), https://pubs.aip.org/aip/jcp/article-pdf/doi/10.1063/5.0005082/16721881/154105_1.online.pdf.
- [68] Ivan Carnimeo, Fabio Affinito, Stefano Baroni, Oscar Basergio, Laura Bellentani, Riccardo Bertossa, Pietro Davide Delugas, Fabrizio Ferrari Ruffino, Sergio Orlandini, Filippo Spiga, and Paolo Giannozzi, “Quantum espresso: One further step toward the exascale,” *Journal of Chemical Theory and Computation* **19**, 6992–7006 (2023), pMID: 37523670, <https://doi.org/10.1021/acs.jctc.3c00249>.
- [69] Xuecheng Shao, Aniket Mandal, Oliviero Andreussi, Davide Ceresoli, Matthew Truscott, Andrew Baczewski, Quinn Campbell, and Michele Pavanello, “QEpy: Quantum ESPRESSO in Python,” (2025), <https://github.com/Quantum-MultiScale/QEpy>.
- [70] W Jones and W H Young, “Density functional theory and the von weizsacker method,” *Journal of Physics C: Solid State Physics* **4**, 1322 (1971).
- [71] Zh. A. Moldabekov, M. Bonitz, and T. S. Ramazanov, “Theoretical foundations of quantum hydrodynamics for plasmas,” *Physics of Plasmas* **25**, 031903 (2018).
- [72] Zhandos Moldabekov, Tim Schoof, Patrick Ludwig, Michael Bonitz, and Tlekkabul Ramazanov, “Statically screened ion potential and Bohm potential in a quantum plasma,” *Physics of Plasmas* **22**, 102104 (2015), https://pubs.aip.org/aip/pop/article-pdf/doi/10.1063/1.4932051/13527324/102104_1.online.pdf.
- [73] M. Akbari-Moghanjoughi, “Hydrodynamic limit of wigner-poisson kinetic theory: Revisited,” *Physics of Plasmas* **22**, 022103 (2015).
- [74] Néstor R. Arista and Werner Brandt, “Dielectric response of quantum plasmas in thermal equilibrium,” *Phys. Rev. A* **29**, 1471–1480 (1984).
- [75] Simon Gravel and N. W. Ashcroft, “Nonlinear response theories and effective pair potentials,” *Phys. Rev. B* **76**, 144103 (2007).
- [76] Zhandos A. Moldabekov, Tobias Dornheim, and Michael Bonitz, “Screening of a test charge in a free-electron gas at warm dense matter and dense non-ideal plasma conditions,” *Contributions to Plasma Physics* **62**, e202000176 (2022), <https://onlinelibrary.wiley.com/doi/pdf/10.1002/ctpp.202000176>.
- [77] Zh.A. Moldabekov, S. Groth, T. Dornheim, M. Bonitz, and T.S. Ramazanov, “Ion potential in non-ideal dense quantum plasmas,” *Contributions to Plasma Physics* **57**, 532–538 (2017).
- [78] R. P. Feynman, N. Metropolis, and E. Teller, “Equations of state of elements based on the generalized fermi-thomas theory,” *Phys. Rev.* **75**, 1561–1573 (1949).